CHEMISTRY
A EUROPEAN JOURNAL

DOI: 10.1002/chem.200801077

# Highly Fluorescent Conjugated Pyrenes in Nucleic Acid Probes: (Phenylethynyl)pyrenecarbonyl-Functionalized Locked Nucleic Acids

**Irina V. Astakhova,[a, b] Vladimir A. Korshun,*[a] and Jesper Wengel*[b]**

**Abstract:** In recent years, fluorescently labeled oligonucleotides have become a widely used tool in diagnostics, DNA sequencing, and nanotechnology. The recently developed (phenylethynyl)pyrenes are attractive dyes for nucleic acid labeling, with the advantages of long-wave emission relative to the parent pyrene, high fluorescence quantum yields, and the ability to form excimers. Herein, the synthesis of six (phenylethynyl)pyrene-functionalized locked nucleic acid (LNA) monomers **M$^1$**–**M$^6$** and their incorporation into DNA oligomers is described. Multilabeled duplexes display higher thermal stabilities than singly modified analogues. An increase in the number of phenylethynyl substituents attached to the pyrene results in decreased binding affinity towards complementary DNA and RNA and remarkable bathochromic shifts of absorption/emission maxima relative to the parent pyrene fluorochrome. This bathochromic shift leads to the bright fluorescence colors of the probes, which differ drastically from the blue emission of unsubstituted pyrene. The formation of intra- and interstrand excimers was observed for duplexes that have monomers **M$^1$**–**M$^6$** in both complementary strands and in numerous single-stranded probes. If more phenylethynyl groups are inserted, the detected excimer signals become more intense. In addition, (phenylethynyl)pyrenecarbonyl–LNA monomers **M$^4$**, **M$^5$**, and **M$^6$** proved highly useful for the detection of single mismatches in DNA/RNA targets.

**Keywords:** (phenylethynyl)pyrenes · fluorescent probes · locked nucleic acids · long-wave fluorescence · oligonucleotides

## Introduction

Currently, there is remarkable growth in the use of synthetic oligonucleotide analogues in bioorganic chemistry, medicine, and molecular biology. Thus, fluorescently labeled oligonucleotides have now widely been introduced for the detection and study of nucleic acids in complex environments. Pyrene-based dyes are of increasing interest for these applications because of pyrene's photophysical properties, such as the long lifetime of its excited state, sensitivity towards microenvironmental changes, and propensity to π-stacking.[1] A pyrene label covalently attached to the sugar part of nucleosides has been used for the detection of nucleic acid hybridization.[2] Recently, 2′-amino variants of locked nucleic acid (LNA) derivatives that contain pyrene fluorochrome have been reported (Scheme 1). It has been shown that the bicyclic skeleton of 2′-amino-LNA and a short linkage act to direct hydrophobic pyrene residues into the minor groove of nucleic acid duplexes.[3] Oligonucleotide probes with pyrene–LNA modifications displayed a high affinity towards DNA/RNA complements,[4] high fluorescence quantum yields,[3] remarkable fluorescence energy resonance transfer (FRET) efficiency,[5] an ability to form interstrand excimers,[6] and sensitivity of the pyrene fluorescence to nucleic acid hybridization.[3,7] These properties make these probes a promising tool for homogeneous fluorescence assays[4b–f,5] and Ångström-scale chemical engineering.[6,8]

However, the relatively short absorption wavelengths of pyrene are an obstacle for its use in in vivo experiments because of the cell autofluorescence observed upon excitation at the same wavelengths.[1a,9] This limitation of pyrene can be overcome by altering its chemical functionalization and

[a] I. V. Astakhova, Dr. V. A. Korshun
Shemyakin-Ovchinnikov Institute of Bioorganic Chemistry
Miklukho-Maklaya 16/10
117997 Moscow (Russia)
Fax: (+7) 495-330-6738
E-mail: korshun@mail.ibch.ru

[b] I. V. Astakhova, Prof. Dr. J. Wengel
Nucleic Acid Center
Department of Physics and Chemistry
University of Southern Denmark
5230 Odense M (Denmark)
Fax: (+45) 6-550-4385
E-mail: jwe@ifk.sdu.dk

Supporting information for this article is available on the WWW under http://dx.doi.org/10.1002/chem.200801077.


WILEY InterScience DISCOVER SOMETHING GREAT
© 2008 Wiley-VCH Verlag GmbH & Co. KGaA, Weinheim

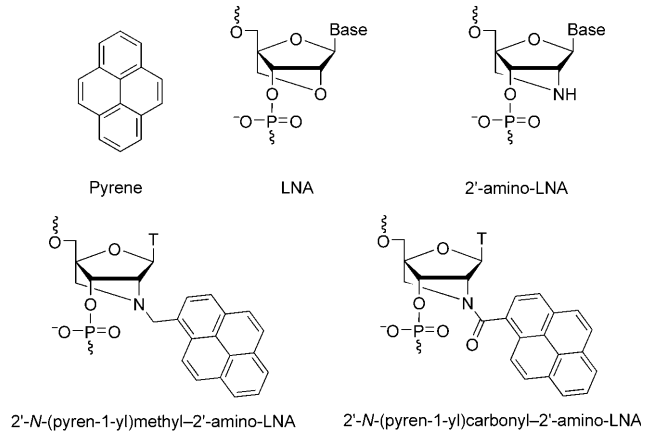


Scheme 1. The chemical structures of the pyrene fluorochrome and LNA, 2′-amino-LNA, and its 1-pyrenemethyl[4b] and 1-pyrenoyl[3] derivatives; T = thymin-1-yl.

thereby affecting the spectroscopic and photophysical properties of the fluorochrome. Recently, the 1-(phenylethynyl)-pyrene (1-PEPy) fluorochrome was introduced as an improved dye for nucleic acid labeling.[9a,10] Thus, the presence of one or more phenylethynyl groups induced an increase in the pyrene's absorption together with a bathochromic shift in the absorption and emission maxima ($\lambda \approx 50$ and 30 nm, respectively), a decrease in the Stokes' shift and excited lifetime, and an increased emission quantum yield. More recently, systematic photophysical evaluations of 1-PEPy, 1,6-bisPEPy, and DP1–DP3 were reported (Scheme 2).[9] Upon incorporation of the second phenylethynyl group, the absorbance and fluorescence maxima of 1,6-bisPEPy were red-shifted by $\lambda \approx 25$ and 30 nm, respectively, compared with monoPEPy, and $\lambda \approx 75$ and 60 nm, respectively, compared with unsubstituted pyrene. In turn, attachment of bulky arylethynyl groups to positions 6 and 8 of the pyrene dimers DP1–DP3 resulted in a ≈45 nm red shift of the fluorescence maxima compared to the reference unsubstituted compound (Scheme 2; R = H). Additionally, compounds DP1–DP3 exhibited high fluorescence quantum yields ($\Phi_F = 0.88$ for DP2 in cyclohexane) and remarkable excimer emission at $\lambda_{max} \approx 525$ nm. The fluorescence quantum yields of 1,6-bisPEPy and 1-PEPy in EtOH were observed to be $\Phi_F = 0.79$ and 0.90, respectively, and the lifetimes of the excited state of 1-PEPy and 1,6-bisPEPy in EtOH were 7.72 ns and 1.65 ns, respectively. Thus, a short excited lifetime implies that PEPy excimers should confirm the preassociation of two PEPy moieties, not just their mutual spacial attainability, which makes PEPy a specified probe of choice for structural studies of biomolecules.[10e]

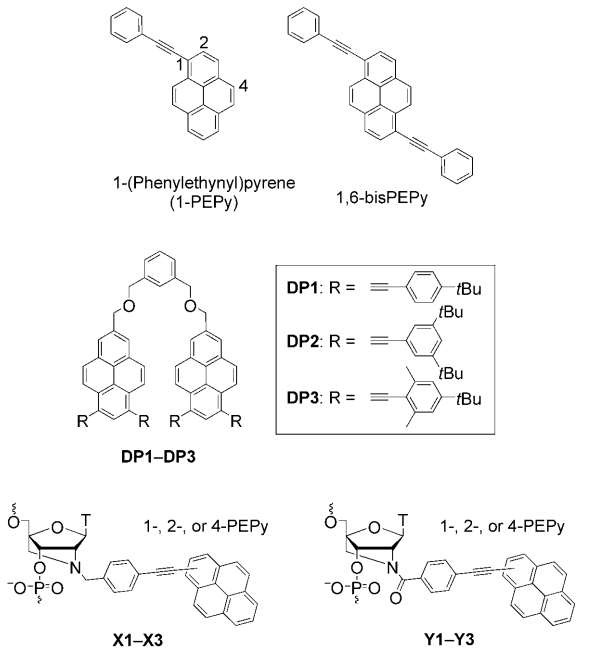


Scheme 2. The chemical structures of 1-PEPy, 1,6-bisPEPy,[9a] DP1–DP3,[9b] and 1-, 2-, and 4-PEPy–LNA monomers **X1**–**X3** and **Y1**–**Y3**;[4e] T = thymin-1-yl.

The high-affinity hybridization of 2′-amino-LNAs functionalized with PEPy has recently been realized, but the spectral and photochemical properties of these conjugates were not thoroughly investigated (Scheme 2, monomers **X1**–**X3** and **Y1**–**Y3**).[4e] Thus, stimulated by the attractive features of modified LNAs[3,4,6–8] and of the PEPy fluorochrome,[9a,10] we have investigated mono-, bis-, and tris(phenylethynyl)pyrene dyes attached to 2′-amino-LNAs at the first or second position of the pyrene nuclei via amide linkage. Herein, we describe the synthesis of mono-, bis-, and tris(phenylethynyl)pyrenecarbonyl (mono-, bis-, and trisPEPyc) LNA monomers (3-phenylethynyl-1-carbonyl (**M**$^{1}$), 6-phenylethynyl-2-carbonyl (**M**$^{2}$), 3,6-bis(phenylethynyl)-1-carbonyl (**M**$^{3}$), 6,8-bis(phenylethynyl)-2-carbonyl (**M**$^{4}$), 3,6,8-tris(phenylethynyl)-1-carbonyl (**M**$^{5}$), 3,6,8-tris(phenylethynyl)-2-carbonyl (**M**$^{6}$)) and their incorporation into DNA oligomers and thermal denaturation studies, and also the spectral properties of conjugates that contain PEPyc moieties positioned either in a probe strand or in each of two complementary strands ("zipper" duplexes).

## Results and Discussion

**Synthesis of PEPyc-modified LNA phosphoramidites**: The general approach to the preparation of PEPy carboxylic acids and their conjugation with 2′-amino-LNA is shown in Schemes 3 and 4, respectively. The bromination of starting 1-acetylpyrene **1** with one or two equivalents of bromine was performed according to the published procedure,[11] with modified temperature and time conditions. Hereby, we obtained mixtures of isomeric bromo products that were used directly in the next step, which was followed by purification of the corresponding PEPy derivatives. The reaction of **1** with three equivalents of bromine at 120 °C[12] resulted in full conversion of the starting compound to tribromopyrene derivative **4**. In turn, mono-, di-, and tri-brominations of isomeric **5**[13] afforded the desired products **6**–**8** in high yields

 © 2008 Wiley-VCH Verlag GmbH & Co. KGaA, Weinheim 

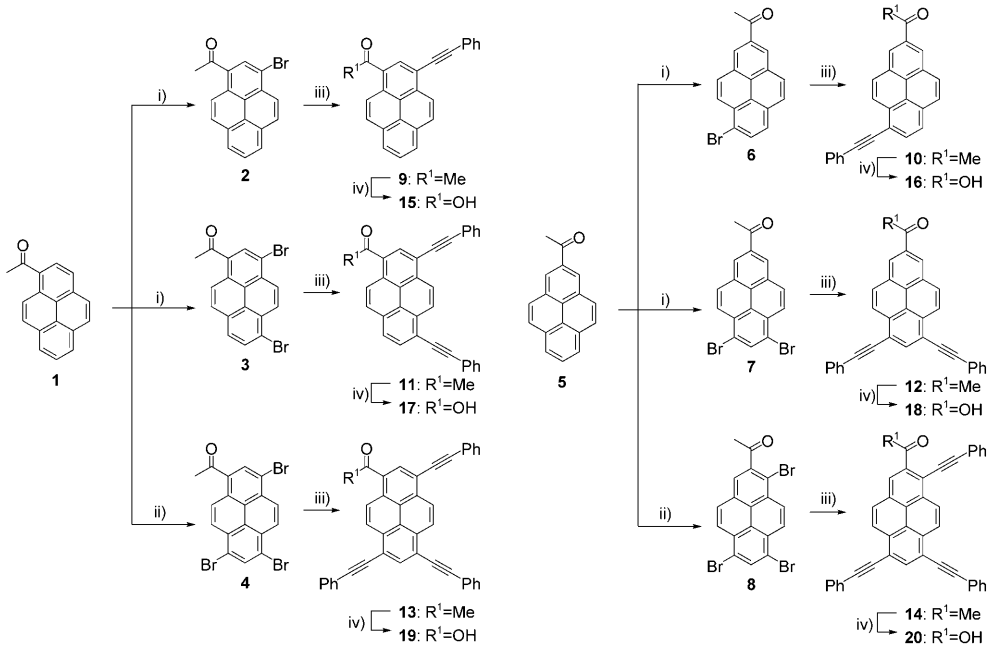

Scheme 3. Synthesis of compounds **9**–**20**. Reagents and conditions: i) $Br_2$, $CCl_4$, 60 °C; ii) $Br_2$, $PhNO_2$, 120 °C; iii) phenylacetylene, $[PdCl_2(PPh_3)_2]$, $PPh_3$, CuI, $NEt_3$, THF, 70 °C; iv) NaOH, $Br_2$, 1,4-dioxane, water, 0 °C.

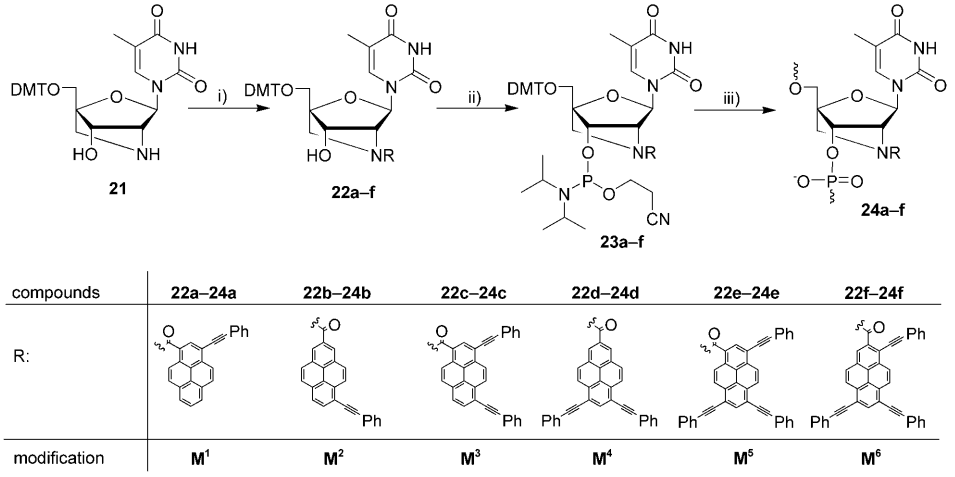

Scheme 4. Synthesis of compounds **22**–**24** from **21**. Reagents and conditions: i) **15**–**20**, HBTU, DIEA, DMF (or DMF-1,1-dichloroethane); ii) $NC(CH_2)_2OP(N(iPr)_2)_2$, diisopropylammonium tetrazolide, $CH_2Cl_2$; iii) DNA synthesizer. DMT = 4,4′-dimethoxytrityl.

under the same conditions as for 1-acetylpyrene. In the case of exhaustive bromination of 2-acetylpyrene, formation of the *ortho* isomer with respect to the acetyl group might take place due to a significant contribution from radicals to the bromination mechanism at high temperature.

The obtained acetylbromopyrenes are prospective building blocks for further modification by a wide range of transition-metal-catalyzed reactions, including possible transformations of the acetyl groups. Phenylethynyl substitution was of interest to us because it would improve the spectroscopic and photophysical properties of the pyrene. Thus, compounds **2**–**4** and **6**–**8** were cross-coupled with phenylacetylene under Sonogashira reaction conditions[14] to give mono-, bis-, and tris-PEPy derivatives **9**–**14**. The yields of compounds **9** and **11** after separation of the isomers were 29% and 53%, respectively, for two steps, whereas the Sonogashira reaction of pure bromopyrenes **4**–**8** resulted in overall yields of 40–80%. The structure of compound **11** was confirmed by HMQC and HMBC NMR spectroscopy. In our strategy, the attachment of PEPy fluorochromes had to be carried out by acylation, and therefore products **9**–**14** were subsequently converted to the corresponding carboxylic acids **15**–**20** under haloform oxidation conditions[15] to prepare for conjugation by amide bond formation.

N2-acylation of 2′-amino-LNA monomer **21**[16] with **15**–**20** was performed in DMF by using HBTU (*O*-(benzotriazol-1-yl)-*N*,*N*,*N*′,*N*′-tetramethyluronium hexafluorophosphate)[17] as the coupling reagent. For compounds **17**–**20**, 1,1-dichloroethane had to be added because of the low solubility of the bis- and trisPEPy acids in DMF. The steric effect of phenylethynyl substituents on the accessibility of the carboxylic group may explain why the highest coupling yield (90%) was obtained for least-hindered **16**, whereas the most-hindered **20** gave a yield of only 42%.

 © 2008 Wiley-VCH Verlag GmbH & Co. KGaA, Weinheim 

Surprisingly, the $^{13}C$ NMR spectra of modified nucleosides **22c–f** did not show signals from the C1′–C5′ and C5″ carbon atoms, whereas the $^{13}C$ NMR spectra of monoPEPyc analogues **22a–b** displayed unusually broad nucleoside peaks. However, $^{13}C$ NMR spectroscopy experiments for derivatives **22c–f**, recorded by using 8192 scans, showed broad signals in the $\delta = 100$–$50$ ppm region that were similar to those in the $^{13}C$ NMR spectra of **22a–b** (Figure S1, Supporting Information) for the corresponding nucleoside carbon atoms. The same effect has been previously reported for 3′,5′-silyl-protected *ara*-uridine-2′-carbamates that contain 1-PEPy.[10e] Thus, attachment of bulky modifications to 2′-amino-LNA results in unusual shielding of nucleoside carbon atoms, in the same way as the presence of large silyl groups and aryl carbamate residues does in *ara*-uridine. However, the nature of this shielding still needs to be clarified.

The nucleoside derivatives **22a–f** were phosphitylated with bis(*N*,*N*-diisopropylamino)-2-cyanoethoxyphosphine in $CH_2Cl_2$ and in the presence of diisopropylammonium tetrazolide to give phosphoramidites **23a–f**.

**Synthesis of modified oligonucleotides (ONs)**: PEPyc-modified LNA monomers **23a–f** were used in automated ON synthesis to prepare a series of modified ONs. The sequences of mixed base 9-mer ONs were similar to those previously designed for studies of pyrene-functionalized LNA.[3,4e,6] In addition, 15-mer ONs were designed based on the reported 13-mer sequence used for the study of 2′-*N*-(pyren-1-yl)carbonyl–2′-amino-LNA.[3]

Synthesis of modified ONs was performed by following standard protocols, except for incorporation of sterically hindered monomers **M$^5$** and **M$^6$**, for which a double coupling procedure with an extended coupling time ($2 \times 30$ min) was used. For all the modified monomers, 1*H*-tetrazole was used as the activator. The resulting stepwise coupling yields of monomers **M$^1$**–**M$^6$**, based on the absorbance of the dimethoxytrityl cation released after each coupling step, were 85–95%. The coupling efficiencies of commercial DNA and LNA amidites varied between 98 and 100%. All ONs were purified by reverse-phase HPLC (RP-HPLC) and their identity confirmed by MALDI-TOF mass spectrometry (Table S1, Supporting Information).

**Hybridization of ONs containing monomers M$^1$–M$^6$ with complementary DNA and RNA**: Thermal denaturation temperatures were determined in medium salt buffer by using 1.0 μM of the two complementary strands, and were compared to the denaturation temperatures of the corresponding unmodified duplexes (Table 1). Except for **ON24**,**ON25**:DNA/RNA and **ON32**,**ON33**:DNA/RNA, the thermal denaturation curves of all the duplexes displayed S-

Table 1. Thermal denaturation temperatures ($T_m$) for duplexes of modified ONs and DNA/RNA complements.[a]

| | 5′→3′ sequence | DNA duplex $T_m$ ($\Delta T_m$/mod)[b] [°C] | RNA duplex $T_m$ ($\Delta T_m$/mod) [°C] |
|---|---|---|---|
| **ON1** | GTG A**M$^1$**A TGC | 20.0 (−8.0) | 19.5 (−6.5) |
| **ON2** | GCA **M$^1$**AT CAC | 21.5 (−6.5) | 24.5 (0.0) |
| **ON3** | GCA TA**M$^1$** CAC | 42.5 (+14.5) | 22.5 (−2.0) |
| **ON4** | GTG A**M$^1$**A **M$^1$**GC | 34.5 (+3.3) | 33.0 (+3.5) |
| **ON5** | GCA **M$^1$**A**M$^1$** CAC | 29.0 (+0.5) | 32.0 (+3.8) |
| **ON6** | GTG A**M$^2$**A TGC | 33.5 (+5.5) | 34.0 (+8.0) |
| **ON7** | GCA **M$^2$**AT CAC | 34.0 (+6.0) | 33.5 (+9.0) |
| **ON8** | GCA TA**M$^2$** CAC | 32.5 (+4.5) | 32.0 (+7.5) |
| **ON9** | GTG A**M$^2$**A **M$^2$**GC | 45.0 (+8.5) | 43.5 (+8.8) |
| **ON10** | GCA **M$^2$**A**M$^2$** CAC | 43.5 (+7.8) | 43.5 (+9.5) |
| **ON11** | GTG A**M$^3$**A TGC | 25.0 (−3.0) | <10 (>−16) |
| **ON12** | GCA **M$^3$**AT CAC | <10 (>−18) | 24.0 (−0.5) |
| **ON13** | GCA TA**M$^3$** CAC | 41.0 (+13.0) | <10 (>−14) |
| **ON14** | GTG A**M$^3$**A **M$^3$**GC | >70 (>+21) | 47.5 (+10.8) |
| **ON15** | GCA **M$^3$**A**M** CAC | 42.0 (+7.0) | 37.0 (+6.3) |
| **ON16** | GTG A**M$^4$**A TGC | 32.5 (+4.5) | 30.0 (+4.0) |
| **ON17** | GCA **M$^4$**AT CAC | 28.0 (0.0) | 29.0 (+5.5) |
| **ON18** | GCA TA**M$^4$** CAC | 23.0 (−3.0) | 23.0 (−1.5) |
| **ON19** | GTG A**M$^4$**A **M$^4$**GC | 44.5 (+8.3) | 40.5 (+7.3) |
| **ON20** | GCA **M$^4$**A**M$^4$** CAC | 37.0 (+4.5) | 33.0 (+4.3) |
| **ON21** | GTG A**M$^5$**A TGC | <10 (>−18) | <10 (>−16) |
| **ON22** | GCA **M$^5$**AT CAC | <10 (>−18) | <10 (>−14) |
| **ON23** | GCA TA**M$^5$** CAC | <10 (>−18) | <10 (>−14) |
| **ON24** | GTG A**M$^5$**A **M$^5$**GC | n.t. | n.t. |
| **ON25** | GCA **M$^5$**A**M$^5$** CAC | n.t. | n.t. |
| **ON26** | CG$^L$TTT$^L$A T$^L$A**M$^5$** AT$^L$C A$^{Me}$C$^L$G | 44.0 (−11.5) | 54.5 (−7.5) |
| **ON27** | CG$^L$TTT$^L$A **M$^5$**A**M$^5$** AT$^L$C A$^{Me}$C$^L$G | 32.5 (−9.0) | 45.0 (−6.0) |
| **ON28** | CG$^L$TT**M$^5$**AT$^L$AT$^L$ A**M$^5$**C A$^{Me}$C$^L$G | 42.0 (−4.3) | 34.0 (−11.5) |
| **ON29** | GTG A**M$^6$**A TGC | 30.5 (+2.5) | <10 (>−16) |
| **ON30** | GCA **M$^6$**AT CAC | <10 (>−18) | <10 (>−14) |
| **ON31** | GCA TA**M$^6$** CAC | 32.0 (+4.0) | <10 (>−14) |
| **ON32** | GTG A**M$^6$**A **M$^6$**GC | n.t. | n.t. |
| **ON33** | GCA **M$^6$**A**M$^6$** CAC | n.t. | n.t. |
| **ON34** | CG$^L$TTT$^L$AT$^L$A**M$^6$** AT$^L$C A$^{Me}$C$^L$G | 54.0 (−1.5) | >70 (>+8) |
| **ON35** | GTG ATA TGC | 28.0 | 26.0 |
| **ON36** | GCA TAT CAC | 28.0 | 24.5 |
| **ON37** | CG$^L$TTT$^L$AT$^L$AT AT$^L$C A$^{Me}$C$^L$G | 55.5 | 62.0 |
| **ON38** | CG$^L$TTT$^L$A TAT AT$^L$C A$^{Me}$C$^L$G | 50.5 | 57.0 |
| **ON39** | CG$^L$TTTAT$^L$AT$^L$ ATC A$^{Me}$C$^L$G | 50.5 | 57.0 |

[a] T$^L$ = thymin-1-yl LNA monomer, $^{Me}$C$^L$ = 5-methylcytosin-1-yl LNA monomer, G$^L$ = guanin-9-yl LNA monomer; see Scheme 4 for the structures of monomers **M$^1$**–**M$^6$**. n.t. = no clear melting transition detected by UV melting experiment. [b] $T_m$ values were measured as the maximum of the first derivatives of the melting curves ($A_{260}$ vs. temperature), and reported $T_m$ values are the average of at least two measurements. All $T_m$ values were recorded in medium salt buffer. $\Delta T_m$/mod: the change in $T_m$ per modification relative to the corresponding reference duplex).


© 2008 Wiley-VCH Verlag GmbH & Co. KGaA, Weinheim

shaped monophasic transitions similar to those of the unmodified reference duplexes (Figure S2, Supporting Information). In the case of **ON24**, **ON25**, **ON32**, and **ON33**, formation of duplexes with DNA and RNA complements was confirmed by fluorescence spectroscopy and circular dichroism (CD).

Previously, it was reported that insertion of an unsubstituted 2′-amino-LNA monomer into a 9-mer mixed-base sequence induces a significant increase in the thermal stability of duplexes with both complementary DNA and RNA.[4a] Conjugation of the pyrene to 2′-amino-LNA by a short rigid amide linker does not decrease binding affinity of the ONs due to a double helix geometry that allows accommodation of the polyaromatic group in the minor groove of the duplexes.[3] However, monomer $\mathbf{M^1}$ showed a destabilizing effect, except for an extraordinarily high stabilization in the case of the **ON3**:DNA duplex ($\Delta T_m$/mod = +14.5 °C). Perhaps the presence of a phenylethynyl group in $\mathbf{M^1}$ that is close to the site of attachment of PEPy to 2′-amino-LNA causes difficulties for accommodation of the modification in the narrow minor groove of the resulting duplexes. Additionally, DNA:RNA hybrids, and especially LNA-modified ones, are duplexes of the A/B transition type.[18] This implies alterations of the double-helix parameters from the pure B-type, such as widening of the minor groove, which correlates with the higher $T_m$ values of $\mathbf{M^1}$-modified DNA:RNA duplexes.

Insertion of two $\mathbf{M^1}$ monomers results in increased binding affinity of ONs towards both complementary DNA and RNA, which suggests a stabilizing interaction between PEPy residues in the complementary complexes (Table 1; data for the duplexes of **ON4** and **ON5** with DNA/RNA complements). This interaction might arise due to the spatial preassociation of two pyrene residues in the duplex. Additionally, replacement of modification $\mathbf{M^1}$ with isomeric, less sterically hindered $\mathbf{M^2}$ in a 9-mer mixed-base sequence resulted in thermal stabilities of the same magnitude as for 2′-*N*-(pyren-1-yl)carbonyl–2′-amino-LNAs (Table 1; data for **ON6**–**ON8**:DNA/RNA).[3]

If the number of phenylethynyl substituents attached to the pyrene core is increased, the singly labeled duplexes formed with both complementary DNA and RNA are dramatically destabilized, which most likely results from the distortion of the double helix geometry by the bulky modifications $\mathbf{M^3}$, $\mathbf{M^5}$, and $\mathbf{M^6}$ (Table 1; $T_m$ values for **ON11**, **ON12**, **ON21**–**ON23**, and **ON29**–**ON31** towards DNA/RNA complements). Interestingly, a $\mathbf{M^3}$-modified duplex with a constitution analogous to that of **ON3**:DNA displayed a remarkable stabilizing effect as well, which was probably due to the intercalation of the modifications into the double helix (Table 1, **ON13**:DNA). It is worth noting that duplexes that contain $\mathbf{M^4}$ display higher thermal denaturation temperatures than those that contain $\mathbf{M^3}$, $\mathbf{M^5}$, and $\mathbf{M^6}$, which might be explained by less steric hindrance from modification $\mathbf{M^4}$. Furthermore, duplexes with two insertions of $\mathbf{M^3}$ or $\mathbf{M^4}$ exhibit impressive increases in the thermal denaturation temperatures compared with singly modified analogues, which underlines an effective communication between PEPy groups in the double stranded constructs (Table 1; e.g., duplexes of **ON14**, **ON15**, **ON19**, and **ON20** with DNA/RNA complements, compared with the duplexes formed by **ON11**–**ON13** and **ON16**–**ON18**). In turn, thermal denaturation curves of duplexes that contain two insertions of $\mathbf{M^5}$ or $\mathbf{M^6}$ do not exhibit a clear melting transition, whereas CD spectra of the single-stranded probes and the corresponding duplexes are rather similar (Figure S9H, Supporting Information). This suggests that interaction between two PEPyc monomers might stabilize single-stranded helical conformation of the doubly $\mathbf{M^5}$ or $\mathbf{M^6}$-labeled ONs, which resembles the conformation of the probes within the duplexes.

**Hybridization of ONs containing monomers $\mathbf{M^1}$–$\mathbf{M^6}$ with mismatched DNA and RNA**: In addition, we evaluated the Watson–Crick selectivity of singly modified probes **ON16**, **ON26**, and **ON34** towards DNA and RNA strands that contained a single mismatched nucleotide at the central three positions (Table 2). Probe **ON16** exhibits excellent mismatch discrimination, except against its DNA target with mismatched nucleotides at position 6. In this case, the thermal stability of the mismatched duplexes is similar to or higher than the one for fully matched duplex **ON16**:DNA. This suggests that the presence of mismatched nucleotides directly opposite monomer $\mathbf{M^4}$ might promote an intercalation of the PEPy residue into the duplexes. At the same time, probe **ON16** does not bind to any other mismatched DNA/RNA targets at temperatures above 10 °C, which makes it a promising tool for mismatch-sensitive nucleic acid detection.

As expected, longer sequences **ON26** and **ON34**, which contain five affinity-enhancing LNA monomers, bind complementary DNA and RNA more strongly and are thus less mismatch-selective than **ON16** (Table 2; $T_m$ values for **ON26** and **ON32** against complementary and singly mismatched DNA/RNA, compared with duplexes of **ON16**). Nevertheless, the presence of mismatches decreases the thermal denaturation temperatures of the complexes compared with the corresponding fully matched duplexes. Probe **ON34** containing monomer $\mathbf{M^6}$ showed better mismatch discrimination relative to $\mathbf{M^5}$-modified analogue **ON26**, and both **ON26** and **ON34** exhibit the best Watson–Crick discrimination of DNA targets with mismatched nucleotides at position 10. This is in disagreement with previously reported data that shows that mismatches opposite the LNA monomers are more efficiently discriminated against than those opposite unmodified nucleotides.[19] For RNA targets, probe **ON26** showed the best Watson–Crick discrimination with mismatches that were opposite modification $\mathbf{M^5}$ (position 9). In turn, single mismatches at positions 8–10 of the RNA target were all equally well discriminated by probe **ON32**, as demonstrated by a decrease in $T_m$ values of more than 15 °C.

**Spectral and photophysical properies of PEPyc-modified oligomers and their duplexes with complementary DNA and RNA**: The UV/Vis absorption and steady-state fluorescence emission spectra were obtained in medium salt buffer with

 © 2008 Wiley-VCH Verlag GmbH & Co. KGaA, Weinheim 

Table 2. Thermal denaturation temperatures for duplexes of **ON19**, **ON26**, and **ON32** and their DNA/RNA complements with single mismatches.[a]

| | ON:target[b] | $T_m$ [°C] | | | | | | | |
|---|---|---|---|---|---|---|---|---|---|
| | | DNA target, **B**: | | | | RNA target, **B**: | | | |
| | | A | C | G | T | A | C | G | U |
| ON16 target | 5′-GTG AM[4] ATGC<br>3′-CAC BAT ACG | <10 | <10 | <10 | **32.5** | <10 | <10 | <10 | **30.0** |
| | 5′-GTG AM[4] ATGC<br>3′-CAC TBT ACG | **32.5** | 33.0 | 33.0 | 36.0 | **30.0** | <10 | <10 | <10 |
| | 5′-GTG AM[4] ATGC<br>3′-CAC TAB ACG | <10 | <10 | <10 | **32.5** | <10 | <10 | <10 | **30.0** |
| ON26 target | 5′-CG[L]TTT[L]AT[L]AM[5] AT[L]CA[Me]C[L]G<br>3′-GCA AAT ABA TAG TGC | 40.5 | 43.0 | 41.5 | **44.0** | 51.0 | 50.0 | 52.5 | **54.5** |
| | 5′-CG[L]TTT[L]AT[L]AM[5] AT[L]CA[Me]C[L]G<br>3′-GCA AAT ATB TAG TGC | **44.0** | 41.0 | 44.0 | 42.0 | **54.5** | 48.0 | 47.0 | 47.5 |
| | 5′-CG[L]TTT[L]AT[L]AM[5] AT[L]CA[Me]C[L]G<br>3′-GCA AAT ATA BAG TGC | 34.0 | 37.0 | 36.0 | **44.0** | 50.0 | 48.5 | 49.0 | **54.5** |
| ON32 target | 5′-CG[L]TTT[L]AT[L]AM[6] AT[L]CA[Me]C[L]G<br>3′-GCA AAT ABA TAG TGC | 43.5 | 43.5 | 45.0 | **54.0** | 53.0 | 53.0 | 55.0 | >**70** |
| | 5′-CG[L]TTT[L]AT[L]AM[6] AT[L]CA[Me]C[L]G<br>3′-GCA AAT ATB TAG TGC | **54.0** | 47.0 | 47.0 | 48.5 | >**70** | 51.0 | 52.5 | 52.5 |
| | 5′-CG[L]TTT[L]AT[L]AM[6] AT[L]CA[Me]C[L]G<br>3′-GCA AAT ATA BAG TGC | 41.0 | 44.5 | 45.0 | **54.0** | 51.5 | 51.0 | 53.0 | >**70** |

[a] For the conditions of the thermal denaturation experiments, see Table 1; the melting temperatures of fully matched duplexes are shown in bold. The melting temperatures of unmodified duplexes are 28.0 and 26.0 °C for **ON16**:DNA and **ON16**:RNA, respectively, and 55.5 and 62.0 °C for **ON26**(**ON32**):DNA and **ON26**(**ON32**):RNA, respectively. [b] DNA targets are shown. RNA targets have the same sequences and contain U nucleosides instead of T.

0.1–1.0 μM of the single stranded probe or the two complementary strands. For recording fluorescence spectra, excitation wavelengths of $\lambda = 375$ (**M[1]**), 370 (**M[2]**), 415 (**M[3]**), 395 (**M[4]**), 425 (**M[5]**), and 420 nm (**M[6]**) were used. Fluorescence emission quantum yields of PEPyc-modified ONs and duplexes were determined relative to reference standards. A highly diluted solution of 9,10-diphenylanthracene ($\Phi_F = 0.95$)[20] in cyclohexane was the first reference standard. The fluorescence quantum yields of 5-(pyren-1-ylethynyl)-2′-deoxyuridine[21] in ethanol and perylene ($\Phi_F = 0.93$)[22] in cyclohexane were measured to be $\Phi_F = 0.45$ and 0.93, respectively, relative to the first standard. The optical densities of the solutions used for quantum yield measurements were kept between 0.1–0.01 to avoid uncertainties. The $\Phi_F$ values were corrected with the refractive index of the solvents. The quantum yields of several samples were also measured in degassed buffer solutions, but no significant difference was found when compared with nondegassed solutions. Thus, all the $\Phi_F$ values presented were determined for air-saturated solutions.

Table 3 lists the spectral and photophysical properties of the **M[1]**–**M[4]**-functionalized ONs (SSP) and their duplexes with DNA and RNA complements. All the UV/Vis spectra for monoPEPyc monomers **M[1]** and **M[2]** contain two main absorption bands near the visible region, with $\lambda_{max} \approx 391$–399 and 369–381 nm. Absorbances by **M[2]**-containing ONs are blue-shifted by ≈5 nm relative to **M[1]**-containing ONs, and both modifications display a 1–5 nm shift in $\lambda_{max}$ upon hybridization to complementary DNA, but not RNA. The absorption maxima are slightly redshifted and the absorption coefficients increase with increasing number of incorporated monomers **M[1]** and **M[2]**. There is a minor difference in the excitation spectra obtained for ONs and duplexes that contain monomers **M[1]** and **M[2]** compared to their absorbance spectra (Figure S3, Supporting Information).

The fluorescence spectra of ONs and duplexes that contain single insertions of **M[1]** and **M[2]** lie within the $\lambda = 400$–480 nm region, and none of them exhibit significant vibrational features (Figure S4, Supporting Information). The Stokes' shift for monoPEPyc monomers is ≈25 nm. Singly labeled **ON1** and **ON6** reveal a broad unstructured band at $\lambda_{max} \approx 430$ nm, which slightly shifts (1–4 nm) to shorter wavelengths upon hybridization. If the emission spectra of single-stranded probes are compared with those of the corresponding duplexes, no perceptible changes in the shape of the spectral curves or the fluorescence intensities are observed. Doubly modified **ON9** displays a broad, unstructured band of excimer emission at $\lambda_{max} \approx 490$ nm, which does not appear upon hybridization with DNA/RNA complements (Figure S4, Supporting Information). However, excimer formation is not taking place in the case of **M[1]**-mofidied **ON4**. Although excimer emission is not observed, there might be an-

Table 3. Spectroscopic and photophysical properties of modified ONs and duplexes that contain monomers **M[1]**–**M[4]**.

| | $\lambda_{abs}^{max}$ bands I, II [nm] | | | $\lambda_{fl}^{max}$ [nm] | | | $\Phi_F$ | | | FB[a] | | |
|---|---|---|---|---|---|---|---|---|---|---|---|---|
| | SSP[b] | DNA | RNA | SSP | DNA | RNA | SSP | DNA | RNA | SSP | DNA | RNA |
| **ON1** | 398, 378 | 394, 379 | 397, 379 | 423 | 422 | 424 | 0.43 | 0.39 | 0.32 | 18.7 | 25.4 | 18.0 |
| **ON4** | 399, 381 | 397, 376 | 398, 378 | 444 | 425 | 425 | 0.09 | 0.09 | 0.07 | 5.1 | 5.4 | 5.2 |
| **ON6** | 393, 372 | 390, 369 | 393, 373 | 423 | 420 | 419 | 0.27 | 0.45 | 0.28 | 14.9 | 26.6 | 22.4 |
| **ON9** | 397, 375 | 392, 370 | 391, 370 | 417 | 418 | 418 | 0.07 | 0.08 | 0.08 | 4.6 | 4.6 | 4.6 |
| **ON11** | 435, 413 | 435 | n.d.[c] | 443 | 443 | n.d. | 0.65 | 0.39 | n.d. | 32.8 | 27.1 | n.d. |
| **ON14** | 433, 413 | 428 | 432, 419 | 452 | 466 | 453 | 0.11 | 0.04 | 0.03 | 6.2 | 2.9 | 1.8 |
| **ON16** | 414, 395 | 417, 396 | 408, 391 | 425 | 427 | 423 | 0.21 | 1.00 | 0.75 | 8.8 | 33.0 | 22.6 |
| **ON19** | 411, 392 | 410, 392 | 403, 388 | 500 | 422 | 420 | 0.07 | 0.03 | 0.03 | 5.9 | 2.0 | 1.8 |

[a] FB = fluorescence brightness FB = $\varepsilon_{425} \times \Phi_F$. [b] SSP = Single-strand probe. [c] n.d. = no duplex formed above 10 °C; see Table 1.[3]

 © 2008 Wiley-VCH Verlag GmbH & Co. KGaA, Weinheim 

other mechanism of fluorescence quenching that results in the reduced quantum yields of **ON4** and its duplexes (e.g., interaction with nucleobases). It is also worth noting that the fluorescence spectrum of single-stranded **ON4** is entirely redshifted by 19 nm with regard to **ON4**:DNA/RNA. At the same time, the fluorescence quantum yields of ONs and duplexes with single incorporations of $\mathbf{M^1}$ or $\mathbf{M^2}$ are remarkably higher than typical quantum yields[23] of pyrene on DNA (Table 3; data for **ON1**, **ON6**, and the corresponding duplexes). The high quantum yields measured for PEPyc–LNAs can be explained by the decreased lifetime of the excited state accompanied by the direction of the functionalities attached to 2′-amino-LNA by an amide linker to the minor groove of the nucleic acid helix, thus reducing the quenching of fluorescence.[3,4,24]

As can be seen from data presented in Table 3, expansion of the π-system of pyrene by two phenylethynyl groups has a significant effect on its spectral and photophysical properties. Thus, there is a complete shift in both the absorption maxima to the visible region on going from mono- to bisPEPyc modifications. The absorption bands of ONs and duplexes with monomer $\mathbf{M^3}$ are observed at $\lambda_{max} \approx 433$–435 and 413–419 nm, and at ≈20 nm shorter wavelengths for $\mathbf{M^4}$-modified analogues. Absorbance spectra by the $\mathbf{M^3}$ conjugates are faintly affected by hybridization, whereas the maxima of the $\mathbf{M^4}$ ones are 5–6 nm blueshifted upon hybridization with RNA. As expected, the emission shifts to longer wavelengths on increasing the number of attached phenylethynyl groups, whereas the Stokes' shifts are decreased from $\lambda = 25$ nm for monoPEPyc to $\lambda = 8$ nm for bisPEPyc modifications. Similarly to $\mathbf{M^1}$- and $\mathbf{M^2}$-modified ONs and duplexes, there is a minor difference between the excitation spectra obtained for $\mathbf{M^3}$- and $\mathbf{M^4}$-modified ONs and duplexes compared with their absorbance spectra (Figure S3, Supporting Information).

Singly modified **ON11** and **ON11**:DNA conjugates display essential superiority in their fluorescence quantum yields and fluorescence brightness compared with monoPEPyc monomers. However, in the same manner as described above, insertion of a second $\mathbf{M^3}$ monomer leads to quenched structureless fluorescence and decreased fluorescence quantum yields of single-stranded probes and duplexes (Table 3; data for **ON14**, **ON19**, and their duplexes with complementary DNA and RNA). Interestingly, this correlates with the higher thermal stabilities of the doubly modified duplexes relative to the singly modified ones (Table 1). Additionally, the fluorescence spectra of $\mathbf{M^3}$- and $\mathbf{M^4}$-containing conjugates have a shoulder ($\lambda_{max} \approx 468$ and 450 nm, respectively) that is less clear for isomeric monomer $\mathbf{M^3}$.

If incorporated once in ONs and duplexes, monomer $\mathbf{M^4}$ displays the same emission wavelengths as monoPEPyc fluorochrome $\mathbf{M^1}$ ($\lambda_{max} \approx 420$ nm). The fluorescence intensity of **ON16** at $\lambda = 415$ nm is found to be about 3 times and 3.6 times increased upon hybridization with RNA and DNA complements, respectively, and the fluorescence quantum yields of the resulting **ON16**:DNA and **ON16**:RNA duplexes are extraordinarily high ($\Phi_F = 1.00$ and 0.75, respectively; Figure S5, Supporting Information). However, the emission spectra of ONs and duplexes with double insertions of $\mathbf{M^4}$ are similar to those of **ON14** and its duplexes (spectra are not shown).

As mentioned above, probe **ON16** displays remarkable Watson–Crick selectivity for singly mismatched DNA and RNA targets. Therefore, there are no duplexes formed above 10 °C for all the targets except for DNA strands that contain mismatches at position 6 (Table 2). We recorded the fluorescence spectra of the duplexes, and found that the presence of single mismatches opposite monomer $\mathbf{M^4}$ does not significantly affect fluorescence intensity relative to that of fully matched duplexes (Figure S5E, Supporting Information). Moreover, the fluorescence spectrum of the monomer is seen to be independent of the nature of the mismatch. This might be explained by intercalation of the fluorochrome within a double helix in the presence of a single mismatch. Intercalation might also explain the increased thermal stabilities of the mismatched duplexes compared with the fully matched one.

As described above, single incorporations of $\mathbf{M^5}$ and $\mathbf{M^6}$ into 9-mer ONs dramatically reduces their binding affinity, whereas upon double insertion these monomers result in increased $T_m$ values for the duplexes (Table 1). Singly labeled **ON21**–**23** do not bind to the DNA and RNA complements above 10 °C and, therefore, can be studied by spectroscopy only as single strands. In turn, $\mathbf{M^6}$-modified **ON29** and **ON31** form duplexes with complementary DNA at room temperature and, hence, are characterized by UV/Vis absorption and fluorescence spectroscopy.

The spectral and photophysical properties of the conjugates that contain modifications $\mathbf{M^5}$ and $\mathbf{M^6}$ are collected in Table 4. Representative absorption spectra, steady-state emission spectra and photographs of fluorescence of 9-mer probes singly modified with monomers $\mathbf{M^1}$–$\mathbf{M^6}$ are shown in Figure 1. Absorption bands of ONs that contain trisPEPyc monomers are observed at $\lambda_{max} \approx 449$–461 and 421–435 nm. Modifications $\mathbf{M^4}$–$\mathbf{M^6}$ exhibit an additional absorption band at $\lambda_{max} \approx 310$–340 nm (Figure 1). The spectral broadening at longer wavelengths exhibited by $\mathbf{M^5}$ and $\mathbf{M^6}$ indicates the increments of different vibrational levels of the π-expanded system.[9a] As in the case of $\mathbf{M^1}$–$\mathbf{M^4}$, we observed a slight difference in the excitation spectra for the trisPEPyc monomers compared with their absorbance spectra (Figure S3, Supporting Information).

Fluorescence emission by modifications $\mathbf{M^5}$ and $\mathbf{M^6}$ observed within the $\lambda = 440$–540 nm region (with $\lambda_{max} \approx 465$ nm) revealed the bathochromic shift to be around 100 nm compared to the emission by the parent pyrene.[9a] Such a significant redshift of fluorescence results in bright green and blue emissions by $\mathbf{M^5}$ and $\mathbf{M^6}$, respectively (Figure 1). Insertion of three phenylethynyl groups into the pyrene core also results in an additional emission band at $\lambda_{max} \approx 490$ nm and an even shorter Stokes' shift than observed for bisPEPyc modifications ($\lambda \approx 5$ nm).

Single incorporations of monomers $\mathbf{M^5}$ and $\mathbf{M^6}$ into 9-mer ONs leads to brightly fluorescent probes. In good agreement

 © 2008 Wiley-VCH Verlag GmbH & Co. KGaA, Weinheim 

Table 4. Spectroscopic and photophysical properties of modified ONs and duplexes that contain monomers $\mathbf{M^5}$ and $\mathbf{M^6}$.

| | $\lambda_{abs}^{max}$, bands I, II [nm] | | | $\lambda_{fl}^{max}$ [nm] | | | $\Phi_F$ | | | FB[a] | | |
|---|---|---|---|---|---|---|---|---|---|---|---|---|
| | SSP | DNA | RNA | SSP | DNA | RNA | SSP | DNA | RNA | SSP | DNA | RNA |
| **ON21** | 461, 434 | n.d.[b] | n.d. | 466 | n.d. | n.d. | 0.42 | n.d. | n.d. | 16.7 | n.d. | n.d. |
| **ON24** | 460, 432 | 433 | 432 | 520 | 520 | 520 | 0.02 | 0.04 | 0.04 | 1.6 | 3.2 | 3.2 |
| **ON26** | 456, 428 | 454, 430 | 448, 426 | 468 | 462 | 462 | 0.50 | 0.62 | 0.62 | 21.2 | 37.6 | 41.3 |
| **ON27** | 460, 434 | 454 | 515 | 520 | 515 | 510 | 0.09 | 0.13 | 0.14 | 10.8 | 16.6 | 17.8 |
| **ON28** | 462, 435 | 462, 435 | 461, 434 | 520 | 520 | 520, 66 | 0.20 | 0.20 | 0.27 | 20.5 | 22.6 | 33.9 |
| **ON29** | 455, 428 | 454, 430 | n.d. | 492, 461 | 489, 460 | n.d. | 0.18 | 0.37 | n.d. | 9.1 | 17.7 | n.d. |
| **ON32** | 456, 432 | 435 | 434 | 461 | 520 | 520 | 0.03 | 0.06 | 0.04 | 1.5 | 2.8 | 1.9 |
| **ON34** | 449, 425 | 443, 420 | 441, 421 | 460 | 455 | 456 | 0.14 | 0.59 | 0.65 | 12.2 | 31.9 | 36.9 |

[a] FB = fluorescence brightness FB = $\varepsilon_{425} \times \Phi_F$. [b] n.d. = no duplex formed above 10 °C; see Table 1. [3]

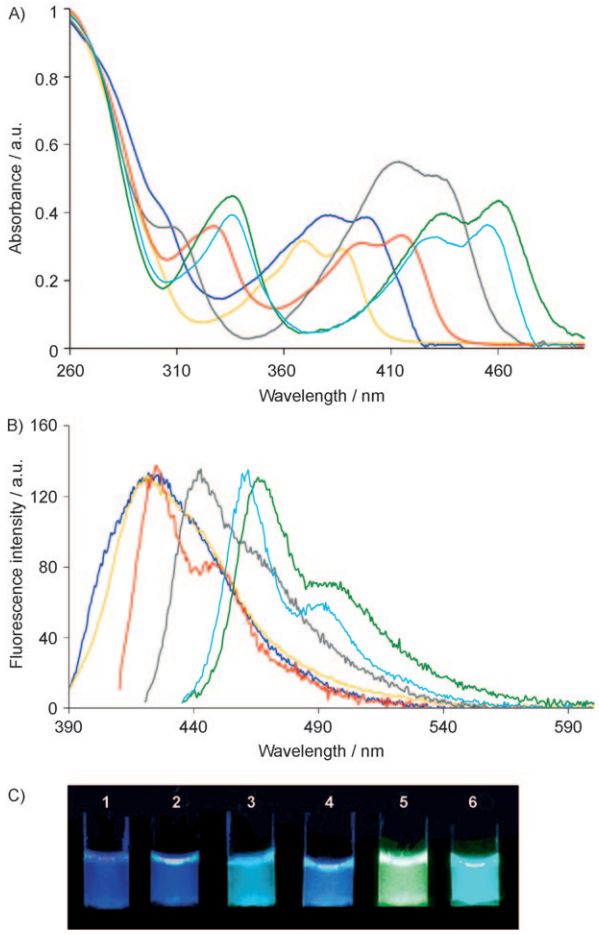


Figure 1. A) Absorption spectra of ONs modified with monomers $\mathbf{M^1}$–$\mathbf{M^6}$ recorded in medium salt buffer at 19 °C with ONs (1.0 μM) and normalized at 260 nm, and B) steady-state emission spectra normalized at the fluorescence maximum, obtained in medium salt buffer at 19 °C with excitation wavelengths of $\lambda = 375$ (**ON1**), 370 (**ON6**), 415 (**ON11**), 395 (**ON16**), 425 (**ON21**), or 420 nm (**ON29**) and 0.1 μM of ONs and complementary strands. For both sets of spectra, ——: **ON1**, ——: **ON6**, ——: **ON11**, ——: **ON16**, ——: **ON21**, ——: **ON29**. C) Photographs of the fluorescence in medium salt buffer of 2.0 μM **ON1** (vial 1), **ON6** (vial 2), **ON11** (vial 3), **ON16** (vial 4), **ON21** (vial 5), and **ON29** (vial 6). Photographs were taken with a digital camera and a laboratory UV lamp ($\lambda_{ex}$ = 365 nm).

with the properties of mono- and bisPEPyc analogues, insertion of a second fluorochrome into 9-mer probes results in dramatic quenching of fluorescence and remarkable excimer formation (Figure S6, Supporting Information). Taking into account the large destabilization effect of $\mathbf{M^5}$ and $\mathbf{M^6}$, we designed 15-mer probes that contained an additional number of affinity-enhancing LNA monomers (Table 1; data for **ON26**–**ON28** and **ON34**). Then we investigated the fluorescence properties of trisPEPyc monomer $\mathbf{M^5}$ incorporated into the 15-mer ONs (Table 4).

Singly modified **ON26** and its duplexes with complementary DNA and RNA exhibit high fluorescence quantum yields ($\Phi_F = 0.50$–$0.65$) and brightness values close to those of the analogues duplexes with four insertions of pyrenecarbonyl–LNA.[3] On the contrary, doubly modified **ON27** shows quenched fluorescence for both the single-stranded probe and its duplexes with DNA/RNA, and this was accompanied by remarkable excimer emission at $\lambda_{max} \approx 520$ nm (Figure S6, Supporting Information). Interestingly, fluorescence spectra of **ON28** and its duplexes show excimer signals as well, even though there are five base pairs separating the PEPyc-modified $\mathbf{M^5}$ nucleotides. Emission of the trisPEPyc excimer reaches $\lambda = 590$ nm, which results in a bright yellow fluorescence of **ON28** and its duplexes. Probably intermolecular stacking between phenyl groups of the PEPyc residues is a key interaction that determines the structural preference of the excimer formation even with a larger distance separating the fluorochromes. At the same time, excimer formation in solution is a diffusion-controlled collision process.[25] Therefore, the increased molecular radii of the PEPyc fluorochromes may significantly affect the rate parameters involved in excimer association and dissociation in solution.

Formation of duplexes with DNA and RNA by the $\mathbf{M^6}$-containing probe **ON34** leads to about a 6-fold increase of the quantum yield (Table 4). Thus, long-wave emission of trisPEPyc fluorochromes attached to 2′-amino-LNA may become a useful tool for the detection of nucleic acid hybridization.

**Fluorescence of PEPy dyes in duplexes of modified ONs with mismatched DNA and RNA**: Owing to the promising fluorescence properties of trisPEPyc monomers, we wanted to apply their long-wave emission for detection of single mismatched nucleotides in DNA and RNA target strands. Thus, we investigated duplexes of probes **ON26** and **ON34** with singly mismatched DNA/RNA complements. The ob-

 © 2008 Wiley-VCH Verlag GmbH & Co. KGaA, Weinheim 

served fluorescence intensities and representative fluorescence spectra are shown in Figure 2. As can be seen, the fluorescence intensity of the duplex **ON26**:DNA is two times greater with the presence of an A:C mismatch at position 8 and two times smaller with a T:G mismatch at position 9. On the contrary, the fluorescence intensity of probe **ON34** is slightly affected by the presence of mismatched nucleotides in the DNA target. As regards duplexes with RNA, **ON26** is seen to be sensitive to A:A, A:C, and T:G mismatches, whereas **ON34** displays the strongest fluorescence in response to a T:G mismatch at position 8 (Figure 2). Thus, the fluorescence of $\mathbf{M}^{5}$- and $\mathbf{M}^{6}$-labeled probes is sensitive to the nature of the neighboring nucleotides and can be used to discriminate matched from mismatched base pairs.

**CD studies with duplexes that contain modifications in one strand**: CD is a convenient method for determination of nucleic acid conformations in solution. Therefore, we employed CD spectroscopy for the structural characterization of modified duplexes. Duplexes **ON1**:DNA and **ON6**:DNA exhibit CD spectra of normal B-type duplexes, which seems to change towards an intermediate A/B form upon hybridization of **ON1** and **ON6** with the RNA complement (Figure S9, Supporting Information).

CD spectra obtained for the duplexes of **ON4** with both DNA and RNA have an additional negative band at $\lambda \approx 300$ nm, which is not observed for either unmodified or singly modified analogues. This suggests that upon double insertion of monomer $\mathbf{M}^{1}$, some preorganized duplex structure might be formed, which also correlates with increased thermal denaturation temperatures and quenched fluorescence of **ON4**:DNA/RNA compared with singly modified **ON1**:DNA/RNA (Table 1, Table 3). CD spectra of 15-mer duplexes **ON26**–**ON27**:DNA/RNA indicate similar conformation to the parent LNA-modified duplexes **ON37**:DNA and **ON37**:RNA (Figure S9, Supporting Information). Hybridization of **ON26** and **ON27** with complementary DNA results in intermediate A/B-type geometry of the duplexes, whereas **ON26**:RNA and **ON27**:RNA exhibit remarkable conformational changes towards the A-form. It is worth noting that the CD spectra are not significantly affected by the introduction of an additional monomer $\mathbf{M}^{5}$ (**ON27**), which suggests successful accommodation of both trisPE-Pyc-modified monomers in the minor groove of the 15-mer duplexes.

**Thermal denaturation studies on zipper duplexes**: Thermal denaturation temperatures of duplexes with two strands each modified by a PEPyc monomer $\mathbf{M}^{1}$–$\mathbf{M}^{6}$ were deter-

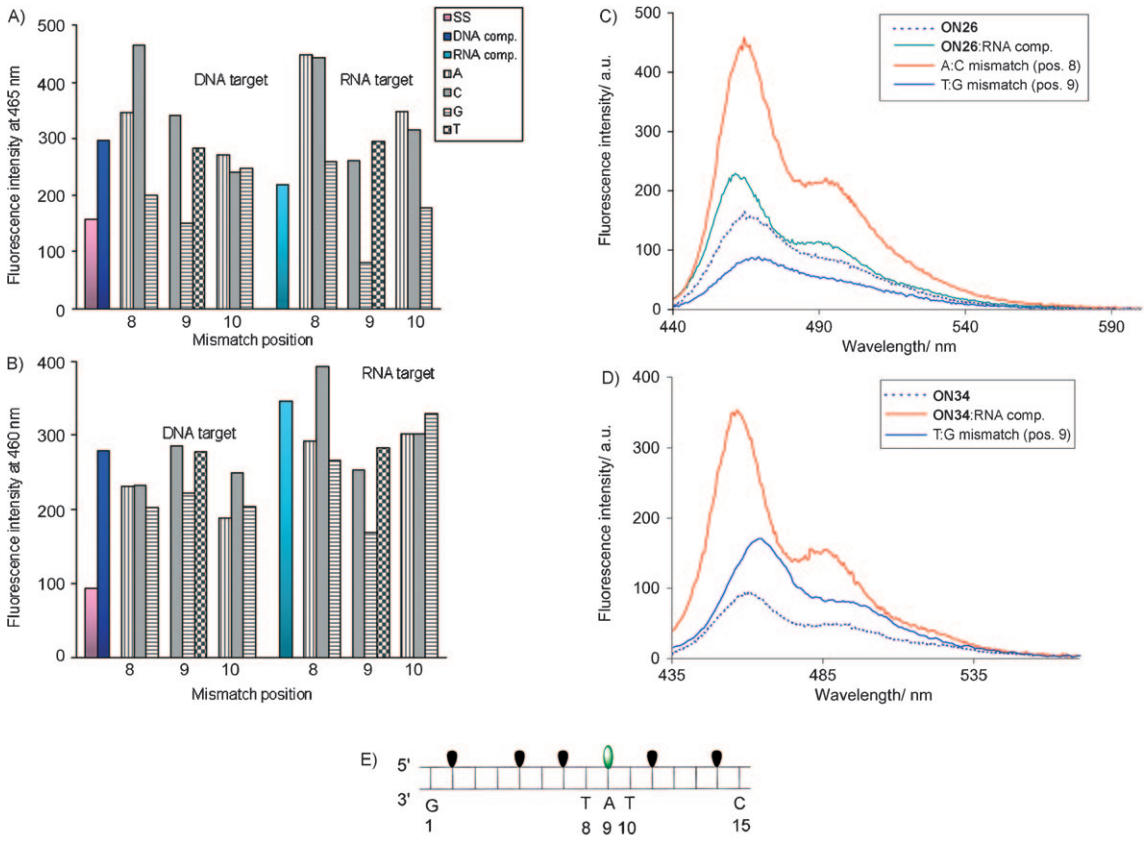


Figure 2. Fluorescence intensities of duplexes between complementary or singly mismatched DNA/RNA targets and A) **ON26** or B) **ON34**. Representative steady-state fluorescence emission spectra of C) **ON26** and D) **ON34** and their duplexes with complementary and singly mismatched DNA. The conditions were as described in Figure 1B. The green and black loops on the zipper schematic indicate $\mathbf{M}^{5}$–$\mathbf{M}^{6}$ and LNA, respectively.


© 2008 Wiley-VCH Verlag GmbH & Co. KGaA, Weinheim

mined as described above. The measured $T_m$ values were compared with those of the corresponding unmodified dsDNA (dsDNA = double-stranded DNA) and are collected in Table 5. In general, the positioning of two modified monomers in various zipper constitutions increase the thermal stabilities compared with duplexes with modifications in one strand only (data presented in Table 5 compared with data in Table 1). For all monomers **M**[1]–**M**[6], the $T_m$ values increase in the order $+1 < -1 < 1+2 < 2+2$ zipper duplexes, which suggests an effective stabilizing interstrand communication between PEPyc functionalities in the created motifs.

Table 5. Thermal denaturation temperatures for modified duplexes with monomers **M**[1]–**M**[6] in both complementary strands.[a]

| | $T_m$ ($\Delta T_m$/mod) [°C] | | | |
|---|---|---|---|---|
| | 5′-d(GTG A**M**A TGC)<br>3′-d(GCA TA**M** CAC) | 5′-d(GTG A**M**A TGC)<br>3′-d(GCA **M**AT CAC) | 5′-d(GTG A**M**A TGC)<br>3′-d(GCA **M**AM CAC) | 5′-d(GTG A**M**A MGC)<br>3′-d(GCA **M**AM CAC) |
| | +1 zipper | −1 zipper | 1+2 zipper | 2+2 zipper |
| **M**[1] | <10 (>−9) | 31.9 (+2.0) | 36.7 (+2.9) | 48.0 (+5.0) |
| **M**[2] | 39.5 (+5.8) | 60.0 (+16.0) | 62.5 (+11.5) | 85.0 (+14.3) |
| **M**[3] | 30.5 (+1.3) | 33.5 (+2.8) | 39.0 (+3.7) | 41.0 (+3.3) |
| **M**[4] | 31.0 (+1.5) | 34.0 (+3.0) | 41.5 (+4.5) | 43.0 (+3.8) |
| **M**[5] | 34.3 (+3.2) | 50.5 (+11.3) | n.t.[b] | n.t. |
| **M**[6] | 36.5 (+4.3) | 40.0 (+6.0) | 40.0 (+4.0) | >70 (>+11) |

[a] Thermal denaturation temperatures were recorded under the same conditions as described in Table 1. The black loops represent monomers **M**[1]–**M**[6]. [b] n.t. = no clear transition.

In addition, we studied thermal stability of +1 and −1 zipper duplexes that contained all possible combinations of monomers **M**[1]–**M**[6] in both complementary strands (Table S2). As for the above-mentioned zipper constructs, the −1 constitution proved to be more stable than the +1 constitution, and for both of them the thermal stability increases as the number of attached phenylethynyl groups increases. Similarly, interstrand communication between **M**[5]-residues in 15-mer zippers (together with incorporation of additional LNA monomers) significantly compensate for the destabilizing effect of the modification (data in Table 6 compared with Table 1; e.g., 44.0 and 66 °C for **ON26**:DNA and **ON26**:**ON41**, respectively).

**Spectral properties of zipper duplexes**: The UV/Vis absorption and steady-state fluorescence emission spectra of the various interstrand zipper arrangements of monomers **M**[1]–**M**[6] were obtained by using the same conditions as described for the ONs and duplexes that contained modifications in one strand. The spectroscopic and photophysical data evaluated for monomers **M**[1]–**M**[6] in +1 and −1 zippers are listed in Table 6. Fluorescence spectra of the various multilabeled duplexes are shown in Figure 3. As one can see, the fluorescence quantum yield of the **M**[1]-containing −1 zipper is of the same magnitude as of the parent **ON1**:DNA (Table 3). All duplexes with monomer **M**[1] in both complementary strands displayed an unstructured monomer emission band at $\lambda_{max} \approx 420$ nm, whereas doubly modified **ON4** exhibits an excimer peak at $\lambda_{max} \approx 500$ nm, which is not detected for −1 and 2+1 zippers (Figure 3A).

Previously, it was reported that the 2+2 zipper arrangement of the pyrene–LNA is the most preferable for the excimer formation compared with the other zippers.[6] Indeed, the 2+2 zipper duplex that contains monomer **M**[1] displayed remarkable excimer formation that correlates with the high thermal denaturation temperature of **ON4**:**ON5**. Incorporation of monomer **M**[2] into the −1 zipper motif resulted in the same quantum yield as for the singly labeled **ON4**:DNA. However, for the +1 zipper analogue the quantum yield was two times lower. It is also worth noting that **M**[2]-modified duplexes displayed more effective excimer formation than the analogous **M**[1]-modified duplexes (Figure 3B). Fluorescence quantum yields of both **M**[3]-containing +1 and −1 zippers were of the same magnitude as for **ON11**:DNA, and both these complexes exhibited intensive monomer emission (Figure 3C). Next, insertion of the third monomer, **M**[3], induced a weak excimer peak, whereas quadruply modified **ON14**:**ON15** showed dramatical quenching of the fluorescence together with ≈1:1 excimer-to-monomer fluorescence intensity ratio (Figure 3C). Double incorporation of **M**[4]-monomers into +/−1 zippers resulted in reduced fluorescence quantum yields for both **ON16**:**ON17** and **ON16**:**ON18** compared with an extraordinarily high quantum yield for **ON16**:DNA ($\Phi_F$ = 1.0). The latter was accompanied by a remarkable excimer

Table 6. Spectroscopic and photophysical properties of duplexes that contain monomers **M**[1]–**M**[6] in +1 zipper and −1 zipper constitutions.[a]

| | 5′ / 3′ | | | | 5′ / 3′ | | | |
|---|---|---|---|---|---|---|---|---|
| | $\lambda_{abs}^{max}$ bands I, II [nm] | $\lambda_{fl}^{max}$ [nm] | $\Phi_F$ | FB[b] | $\lambda_{abs}^{max}$ bands I, II [nm] | $\lambda_{fl}^{max}$ [nm] | $\Phi_F$ | FB[b] |
| **M**[1] | n.d.[c] | n.d. | n.d. | n.d. | 395, 378 | 424 | 0.32 | 30.5 |
| **M**[2] | 391, 369 | 425 | 0.27 | 22.1 | 393, 372 | 427 | 0.41 | 38.5 |
| **M**[3] | 434 | 444 | 0.45 | 58.3 | 433 | 443 | 0.51 | 60.0 |
| **M**[4] | 415, 396 | 520, 424 | 0.37 | 24.5 | 421, 402 | 518 | 0.35 | 25.0 |
| **M**[5] | 457, 435 | 468 | 0.23 | 39.1 | 438 | 468 | 0.23 | 39.2 |
| **M**[6] | 455, 430 | 490, 461 | 0.16 | 16.1 | 450, 432 | 491, 460 | 0.18 | 18.0 |

[a] Thermal denaturation temperatures were recorded under the same conditions as described in Table 1. The black loops represent monomers **M**[1]–**M**[6]. [b] FB = fluorescence brightness FB = $\varepsilon_{425} \times \Phi_F$. [c] n.d. = no duplex formed above 10 °C.[3]

 © 2008 Wiley-VCH Verlag GmbH & Co. KGaA, Weinheim 

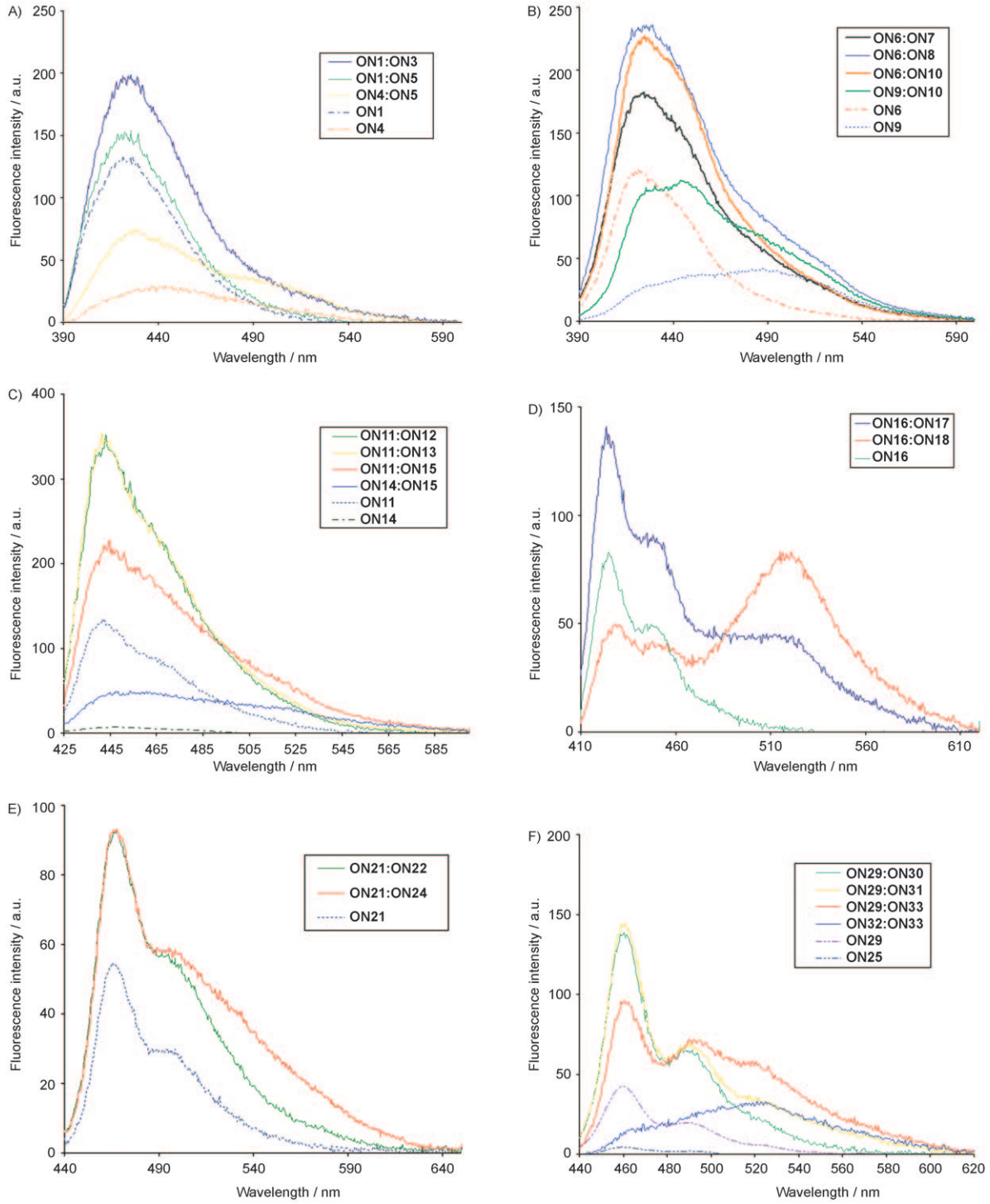


Figure 3. Steady-state fluorescence emission spectra of multilabeled duplexes that contain monomers $\mathbf{M^1}$–$\mathbf{M^6}$ in various zipper constitutions. For conditions, see Figure 1B.

signal at $\lambda_{max} \approx 512$ nm, which is much more intense for the −1 zipper constitution than for the +1 constitution (Figure 3D).

Furthermore, hybridization of $\mathbf{M^5}$- and $\mathbf{M^6}$-modified probes with complementary DNA strands that contained trisPEPyc monomers dramatically decreased the quantum yields, especially in the case of monomer $\mathbf{M^6}$. As for $\mathbf{M^1}$–$\mathbf{M^4}$-modified analogues, the −1 zippers with trisPEPyc fluorochromes exhibit more intensive excimer signals than their +1 analogues (Figure 3D,E). Note that increasing the number of phenylethynyl substitutes attached to the pyrene core leads to more effective interstrand excimer formation

 © 2008 Wiley-VCH Verlag GmbH & Co. KGaA, Weinheim 

(Figure 3; **ON16**:**ON18**, **ON32**:**ON33**, compared with **ON1**:**ON5**, **ON4**:**ON5**).

15-Mer duplexes containing monomer $\mathbf{M^5}$ in both complementary strands showed increasing thermal stabilities and more effective excimer formation in the order **ON26**:**ON40** < **ON26**:**ON41** < **ON27**:**ON40** < **ON27**:**ON41** (Table 5; Figure S7, Supporting Information). Long-wave excimer emission of $\mathbf{M^5}$-modified duplexes exceeds 600 nm, which leads to vivid yellow fluorescence, whereas less redshifted bis- and monoPEPyc excimers result in yellow-green and blue-green solutions, respectively.

Next, we studied PEPyc interstrand excimer formation for combined modifications $\mathbf{M^1}$–$\mathbf{M^6}$ in DNA duplexes of +1 and −1 zipper arrangements. The steady-state fluorescence emission spectra of the duplexes were recorded by using the same conditions as described above, except for the use of excitation wavelengths of $\lambda = 350$ (combinations of mono-/trisPEPyc monomers), 390 (combinations of mono-/bisPEPyc monomers), or 420 nm (combinations of bis-/trisPEPyc monomers); the representative fluorescence spectra of combinarorial zipper duplexes are shown in Figure S8 (Supporting Information). Excimer fluorescence was detected as a broad structureless band at $\lambda_{max} \approx 500$–$530$ nm, whereas monomer emission by combined duplexes was observed at $\lambda_{max} \approx 440$–$460$ nm. We used the excimer-to-monomer fluorescence intensity ratio, $I_{ex}/I_m$, as a criterion of the excimer formation. The resulting $I_{ex}/I_m$ values are presented in Figure 4. As can be seen, the intensity of excimer fluorescence is always higher for combinations of monomers with increased numbers of phenylethynyl groups. The configuration of the −1 zipper is more preferable for excimer formation than that of the +1 zipper, which is in good agreement with the increased thermal denaturation values of −1 zippers relative to +1 zippers (Table S2, Supporting Information). Weak excimer signals were detected for two monoPEPyc monomers $\mathbf{M^1}$ and $\mathbf{M^2}$ in dsDNA, and higher signals for various combinations of $\mathbf{M^4}$, $\mathbf{M^5}$, and $\mathbf{M^6}$. This might be caused by interstrand stacking of phenyl groups that could promote the spatial preorganization of two pyrene residues, and also by the increased molecular radii of bis- and trisPEPyc modifications.

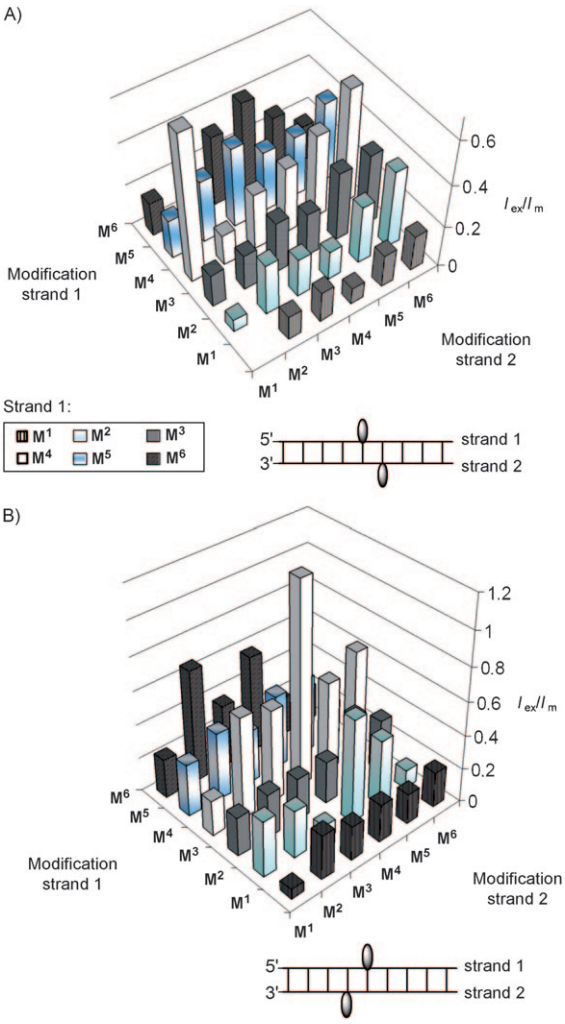


Figure 4. Fluorescent properties of A) +1 and B) −1 zipper duplexes with different combinations of monomers $\mathbf{M^1}$–$\mathbf{M^6}$ in their complementary strands. The spectra were recorded in medium salt buffer at 19 °C with 0.1 μM complementary strands and at the excitation wavelengths mentioned in the text.

## Conclusion

Development of highly emissive fluorochromes for nucleic acid labeling is of considerable interest due to the possibility of their use in both in vitro and in vivo fluorescence assays. Herein, the synthesis of six long-wave emission 2′-(phenylethynyl)pyrenecarbonyl–2′-amino-LNA monomers, $\mathbf{M^1}$–$\mathbf{M^6}$, their incorporation into ONs, their thermal denaturation studies, and their spectral and photophysical properties are described. For the preparation of monomers $\mathbf{M^1}$–$\mathbf{M^6}$, methods for the selective electrophilic mono, di, and tri substitutions of 1- and 2-acetylpyrene were developed by employing transition-metal-catalyzed reactions.

Probes containing phenylethynyl-substituted pyrene monomers $\mathbf{M^1}$–$\mathbf{M^6}$ were demonstrated to be very promising due to significant improvement in the spectral and photophysical characteristics of pyrene. As the number of phenylethynyl substitutuents increases, the absorption/emission maxima are drastically redshifted. This results in the change in the fluorescence colors from purple for monoPEPyc to vivid green and blue for trisPEPyc fluorochromes. At the same time, fluorescence quantum yields and the ability to form excimers were enchanced. Duplexes with a single incorporation of $\mathbf{M^1}$–$\mathbf{M^6}$ display lower thermal stabilities and higher fluorescence quantum yields than their doubly modified analogues. On this basis, we propose an effective electronic interaction between PEPy residues in the multilabeled constructs, which was confirmed by the detection of excimer emission. The fluorescence of a single-stranded probe that contains a single insertion of monomer $\mathbf{M^4}$ is quenched, whereas upon hybridization with complementary DNA and RNA, the fluorescence quantum yields increase up to $\Phi_F = 1.00$ and 0.75, and this accompanied by excellent

 © 2008 Wiley-VCH Verlag GmbH & Co. KGaA, Weinheim 

Watson–Crick mismatch discrimination. Selectivity against singly mismatched DNA/RNA targets is likewise considerable for longer 15-mer ONs that contain **M**$^5$ and **M**$^6$, which in turn display significant changes in fluorescence intensity in the presence of mismatched nucleotides compared with fully matched duplexes. Duplexes with monomers **M**$^1$–**M**$^6$ in both complementary strands revealed remarkable thermal stabilities accompanied by high fluorescence quantum yields and effective excimer formation.

The long-wave emission of these novel probes allows excitation at longer wavelengths without irradiation of intrinsic cell fluorochromes. Taking this advantage into account together with an increased ability to form excimers, sensitivity to the neighboring base pairs, and high fluorescence quantum yields of singly labeled probes, we propose the possibility of applying PEPyc fluorochromes attached to 2′-amino-LNA for both in vitro and in vivo nucleic acid fluorescence assays. Applications of such probes for the in vivo detection of single-nucleotide polymorphisms, fluorescence in situ hybridization including the detection of specific RNAs in living cells, and analysis of gene expression will be especially interesting.

## Experimental Section

**General**: Reagents were obtained from commercial suppliers (Sigma–Aldrich–Fluka) and were used as received; 2-acetylpyrene,[26] 5-(pyren-1-ylethynyl)-2′-deoxyuridine,[21] and diisopropylammonium tetrazolide[27] were synthesized as described. Perylene, 5-(pyren-1-ylethynyl)-2′-deoxyuridine and 9,10-diphenylantracene were used as standards for emission quantum yield measurements after recrystallization. HPLC-grade toluene and acetone were distilled and stored over activated 4 Å molecular sieves. $CH_2Cl_2$ was always freshly distilled over $CaH_2$ before being used. Other solvents were used as received. Photochemical studies were performed with spectroscopy-grade cyclohexane and absolute (abs.) ethanol. NMR spectra were recorded at 303 K by using Varian Gemini 2000 300 MHz and Bruker DRX 500 MHz instruments. Chemical shifts are reported in ppm relative to solvent peaks ($CDCl_3$: 7.26 ppm for $^1$H and 77.0 ppm for $^{13}$C; [D$_6$]DMSO: 2.50 ppm for $^1$H and 39.5 ppm for $^{13}$C; 85% aq. $H_3PO_4$ (external standard): 0.00 ppm for $^{31}$P). $^1$H NMR spectroscopy coupling constants are reported in Hz and refer to apparent multiplicities. ESI mass spectra were obtained by using a Finnigan SSQ 710 mass spectrometer. High-resolution mass spectra were recorded in positive-ion mode by using a IonSpec Fourier Transform ICR mass spectrometer (MALDI) or PESCIEX QSTAR pulsar mass spectrometer (ESI). IR spectra were recorded by using a Perkin–Elmer 1720 infrared fourier transform spectrometer. Melting points were determined by using a Boetius heating table and are uncorrected. Analytical thin-layer chromatography was performed on Kieselgel 60 F254 precoated aluminium plates (Merck). Silica-gel column chromatography was performed by using Merck Kieselgel 60 0.040–0.063 mm. ON synthesis was carried out by using a PerSpective Biosystems Expedite 8909 instrument on a 200 nmol scale with the manufacturer's standard protocols. In the case of LNA phosphoramidites (monomers $T^L$, $G^L$, $^{Me}C^L$), the coupling-step time was extended to 15 min. Additionally, in the case of monomers **M**$^3$–**M**$^6$, a double-coupling procedure was applied. Step-wise coupling yields of 85–95% for monomers **M**$^1$–**M**$^6$ were obtained based on the absorbance of the dimethoxytrityl cation released after each coupling. The coupling efficiencies of standard DNA and LNA amidites varied between 98 and 100%. Cleavage from solid support and removal of nucleobase protecting groups was performed by using standard conditions (32% aqueous ammonia for 12 h at 55°C). Unmodified DNA/RNA strands were obtained from commercial suppliers and used without further purification, and all the modified ONs were purified by using DMT-ON RP-HPLC with the Waters Prep LC 4000 equipped with Xterra MS C18-column (10 μm, 300×7.8 mm). Elution was performed with an initial isocratic hold of A-buffer (95% $NH_4HCO_3$ (0.1 M), 5% $CH_3CN$) for 5 min, followed by a linear gradient to 55% B-buffer (25% $NH_4HCO_3$ (0.1 M), 75% $CH_3CN$) over 75 min at a flow rate of 1.0 mL min$^{-1}$. RP-purification was followed by detritylation (80% aq. AcOH, 20 min), precipitation (abs. EtOH, −18°C, 12 h), and washing three times with abs. EtOH. The identity of ONs was verified by MALDI-TOF mass spectrometry (Table S1, Supporting Information). UV/Vis absorption spectra and thermal denaturation experiments were performed on a Perkin–Elmer Lambda 35 UV/Vis spectrometer equipped with a Peltier Temperature Programmer 6 in a medium salt buffer (NaCl (100 mM), Na-phosphate (10 mM), EDTA (0.1 mM), pH 7.0). The concentrations of ONs were calculated by using the following extinction coefficients ($OD_{260}$/μmol): G 10.5, A 13.9, T/U 7.9, C 6.6, **M**$^1$ 33.5, **M**$^2$ 34.2, **M**$^3$ 31.7, **M**$^4$ 30.2, **M**$^5$ 35.1, **M**$^6$ 34.9. ONs (1.0 μM per strand) were thoroughly mixed, denaturated by heating, and subsequently cooled to the starting temperature of experiment. Thermal denaturation temperatures ($T_m$, °C) were determined to be the maximum of the first derivative of the thermal denaturation curve ($A_{260}$ vs. temperature). Reported $T_m$ values are an average of two measurements within ±1.0°C. Fluorescence spectra were obtained in a medium salt buffer by using a Perkin–Elmer LS 55 luminescence spectrometer equipped with a Peltier temperature controller. For recording fluorescence spectra, 0.1 μM concentrations of the single-stranded probe or corresponding duplex were used. For weakly fluorescent samples the concentration was increased to 0.5 μM. The fluorescence quantum yields were measured by the relative method using 9,10-diphenylantracene ($\Phi_F$=0.95)[20] in cyclohexane as the first standard and 5-(pyrene-1-ylethynyl)-2′-deoxyuridine[21] in abs. EtOH and perylene ($\Phi_F$=0.93)[22] in cyclohexane as the second standard. For fluorescence quantum yield determinations, 0.5μM solutions were used. CD spectra were recorded by using a JASCO J-815 CD spectrometer equipped with a CDF 4265/15 temperature controller.

**General procedure for the monobromination of acetylpyrenes**: A solution of bromine (769 μL, 15 mmol) in $CCl_4$ (25 mL) was added dropwise over 30 min to a stirred solution of the corresponding acetylpyrene (**1** or **5**; 2.44 g, 10 mmol) in $CCl_4$ (50 mL) at RT. After the addition was complete, the mixture was heated to 60°C, kept at this temperature for 1 h, and then allowed to cool to RT to yield a precipitate that was filtered, washed with ethanol (2×30 mL), and dried in vacuo.

*1-Acetyl-3-bromopyrene (**2**)*: The monobromination of **1** resulted in a mixture of isomeric 3-, 6-, and 8-bromopyrenes (yellow solid; 3.05 g, 95%), which was used directly in the next step without further purification. IR (KBr; signals for intense bands are given): $\tilde{\nu}$=3436, 1672, 1587, 1503, 1349, 1235, 846, 713, 674, 632 cm$^{-1}$; ESI-MS (70 eV): *m*/*z* (%): calcd for $C_{18}H_{10}BrO^+$: 321, 322, 323, 324 [$M^+$−H]; found: 321 (100%), 323 (98%), 322 (60%), 324 (22%).

*2-Acetyl-6-bromopyrene (**6**)*: The title compound was obtained as a yellow solid (2.88 g, 90%). $R_f$=0.46 (40% petroleum ether/toluene); m.p. 155–156°C (recrystallized from $PhNO_2$, washed with 96% aq. EtOH); IR (KBr; signals for intense bands are given): $\tilde{\nu}$=3434, 1695, 1590, 1454, 1293, 1169, 1014, 842, 820, 704, 658, 600 cm$^{-1}$; ESI-MS (70 eV): *m*/*z* (%): calcd for $C_{18}H_{10}BrO^+$: 321, 322, 323, 324 [$M^+$−H]; found: 321 (100), 323 (100), 322 (67), 324 (33).

**General procedure for the dibromination of acetylpyrenes**: A solution of bromine (1.28 mL, 25 mmol) in $CCl_4$ (50 mL) was added dropwise over 30 min to a vigorously stirred solution of the corresponding acetylpyrene (2.44 g, 10 mmol) in $CCl_4$ (50 mL) at RT. The reaction mixture was heated to 60°C, kept at this temperature for 6 h, and then cooled to RT to yield a precipitate that was filtered, washed with ethanol (2×30 mL) and dried in vacuo.

*1-Acetyl-3,6-dibromopyrene (**3**)*: The dibromination of **1** resulted in a mixture of isomeric 3,6-, 3,8- and 6,8-dibromoproducts (3.29 g, red solid), which was used directly in the next step without further purification. IR (KBr; signals for intense bands are given): $\tilde{\nu}$=3435, 1682, 1581, 1514, 1365, 1242, 844, 755, 701, 654, 611 cm$^{-1}$; ESI-MS (70 eV): *m*/*z* (%): calcd

 © 2008 Wiley-VCH Verlag GmbH & Co. KGaA, Weinheim 

for $C_{17}H_7Br_2O^+$: 387, 385, 389, 388 [$M^+-CH_3$]; found: 387 (100%), 389 (48%), 385 (43%), 388 (26%).

*2-Acetyl-6,8-dibromopyrene (**7**)*: The title compound was obtained as a yellow solid (3.61 g, 90%). $R_f=0.56$ (40% petroleum ether/toluene); m.p. 218°C (10% EtOH (96% aq.)/$CCl_4$); IR (KBr; signals for intense bands are given) $\tilde{\nu}=3435$, 1698, 1589, 1458, 1291, 1172, 1024, 821, 702, 661 $cm^{-1}$; ESI-MS (70 eV): *m/z* (%): calcd for $C_{18}H_{10}Br_2O^+$: 402, 400, 404, 403 [$M^+$]; found: 400 (100%), 403 (68%), 402 (57%), 404 (37%).

**General procedure for the tribromination of acetylpyrenes**: Bromine (2.05 mL, 40 mmol) was added dropwise under vigorous stirring to a solution of corresponding acetylpyrene (2.44 g, 10 mmol) in nitrobenzene (20 mL) at 120°C over a period of 15 min. The mixture was kept at 120°C for 4 h, then allowed to cool to RT yielding a precipitate, which was filtered, washed with ethanol (2×30 mL) and dried in vacuo.

*1-Acetyl-3,6,8-tribromopyrene (**4**)*: The title compound was obtained as a yellow solid (4.43 g, 92%). $R_f=0.60$ (50% petroleum ether/toluene); m.p. 188–190°C (recrystallized from $PhNO_2$, washed with 96% aq. EtOH); IR (KBr; signals for intense bands are given): $\tilde{\nu}=3435$, 1695, 1596, 1524, 1348, 1227, 1021, 976, 876, 814, 706, 659, 621 $cm^{-1}$; ESI-MS (70 eV): *m/z* (%): 478 (60), 480 (100), 482 (44), 484 (40) [$M^+$].

*2-Acetyl-1,6,8-tribromopyrene (**8**)*: The title compound was obtained as a yellow solid (3.79 g, 79%). $R_f=0.52$ (50% petroleum ether/toluene); m.p. 215–216°C (recrystallized from *o*-dichlorobenzene, washed with 96% aq. EtOH); IR (KBr; signals for intense bands are given) $\tilde{\nu}=3436$, 1722, 1589, 1455, 1283, 1055, 994, 878, 812, 760, 673, 608 $cm^{-1}$; ESI-MS (70 eV): *m/z* (%): 477 (60%), 479 (97%), 481 (100%), 483 (46%) [$M^+-H$].

**General procedure for the Sonogashira coupling of bromopyrenes**: Phenylacetylene, $[PdCl_2(PPh_3)_2]$, $PPh_3$, and CuI were successively added to a degassed solution of the corresponding starting compound in $NEt_3$ (20 mL) and THF (20 mL). The reaction mixture was stirred under argon at 70°C for 16 (**9**, **10**), 24 (**11**, **12**), or 48 h (**13**, **14**). After conversion of the starting material was complete (as monitored by TLC), the mixture was poured into $CHCl_3$ (150 mL). The resulting solution was washed with 3% $Na_2$(edta) (4×100 mL) and water (2×100 mL), dried over $Na_2SO_4$, and evaporated to dryness. The crude products were purified by column chromatography on silica gel as indicated in the individual cases.

*1-Acetyl-3-(phenylethynyl)pyrene (**9**)*: Prepared from **2** (1.29 g, 4 mmol), phenylacetylene (658 μL, 6 mmol), $[PdCl_2(PPh_3)_2]$ (280 mg, 0.4 mmol), $PPh_3$ (210 mg, 0.8 mmol), and CuI (76 mg, 0.4 mmol). The product was purified by column chromatography on silica gel by eluting with 50% $CHCl_3$/petroleum ether. Combined fractions containing the product were evaporated and purified by column chromatography on silica gel by using a gradient elution of 50→70% petroleum ether/toluene to give the product as a yellow solid (426 mg, 29% for two steps). $R_f=0.55$ (5% EtOAc/toluene); m.p. 160°C ($CHCl_3$); $^1$H NMR (500 MHz, $CDCl_3$): $\delta=8.98$ (d, $J=7.6$ Hz, 1H), 8.57 (d, $J=7.6$ Hz, 1H), 8.52 (s, 1H), 8.25–8.18 (m, 2H), 8.17–8.15 (m, 2H), 8.02 (app. t, $J=6.2$ Hz, 1H), 7.74 (d, $J=6.4$ Hz, 2H), 7.49–7.41 (m, 3H), 2.90 ppm (s, 3H); $^{13}$C NMR (500 MHz, $CDCl_3$): $\delta=$ 201.4, 134.2, 131.7 (2C), 131.5, 130.9, 130.8, 130.6, 130.3, 130.2 (2C), 129.3, 128.7, 128.5, 126.9, 126.6, 126.5, 125.2, 124.9, 124.8, 123.9, 123.2, 117.0, 95.5, 87.9, 30.4 ppm; MALDI-HRMS: *m/z* calcd for $C_{26}H_{16}O^+$: 344.1196 [$M^+$]; found 344.1193.

*2-Acetyl-6-(phenylethynyl)pyrene (**10**)*: Prepared from **6** (1.29 g, 4 mmol), phenylacetylene (658 μL, 6 mmol), $[PdCl_2(PPh_3)_2]$ (280 mg, 0.4 mmol), $PPh_3$ (210 mg, 0.8 mmol), and CuI (76 mg, 0.4 mmol). The product was purified by column chromatography on silica gel by using a gradient elution of 50→80% toluene/petroleum ether to give the product as a yellow solid (728 mg, 53%). $R_f=0.39$ (5% EtOAc/toluene); m.p. 140–142°C ($CHCl_3$); $^1$H NMR (300 MHz, $CDCl_3$): $\delta=8.46$ (s, 2H), 8.40 (d, $J=$ 9.0 Hz, 1H), 8.04 (d, $J=8.1$ Hz, 1H), 7.93–7.80 (m, 4H), 7.65 (d, 2H), 7.39–7.36 (m, 3H), 2.77 ppm (s, 3H); $^{13}$C NMR (300 MHz, $CDCl_3$): $\delta=$ 198.3, 134.1, 132.2, 131.7 (2C), 131.5, 130.8, 130.6, 130.4, 128.5 (2C), 128.4 (2C), 128.3, 127.8, 126.2, 126.1, 124.8 (2C), 124.7 (2C), 124.1, 123.8, 95.5, 88.1, 27.0 ppm; MALDI-HRMS: *m/z* calcd for $C_{26}H_{16}O^+$: 344.1196 [$M^+$]; found: 344.1190.

*1-Acetyl-3,6-bis(phenylethynyl)pyrene (**11**)*: Prepared from **3** (1.21 g, 3 mmol), phenylacetylene (988 μL, 9 mmol), $[PdCl_2(PPh_3)_2]$ (421 mg, 0.6 mmol), $PPh_3$ (315 mg, 1.2 mmol), and CuI (114 mg, 0.6 mmol). The product was purified by column chromatography on silica gel by using a gradient elution of 20→80% $CHCl_3$/petroleum ether. The combined fractions containing the product were evaporated and purified by column chromatography on silica gel by using a gradient elution of 40→50% toluene/petroleum ether to give the product as an orange solid (858 mg, 53% for two steps). $R_f=0.63$ (5% EtOAc/toluene); m.p. 195–199°C ($CHCl_3$); $^1$H NMR (300 MHz, $CDCl_3$): $\delta=9.02$ (d, $J=9.6$ Hz, 1H), 8.69 (d, $J=9.6$ Hz, 1H), 8.55 (d, $J=9.0$ Hz, 1H), 8.50 (s, 1H), 8.17–8.09 (m, 3H), 7.68–7.65 (m, 4H), 7.40–7.37 (m, 6H), 2.87 ppm (s, 3H); $^{13}$C NMR (300 MHz, $CDCl_3$): $\delta=201.6$, 134.6, 134.3, 133.9, 132.2, 132.1, 132.0, 131.6, 131.5, 131.3, 131.2, 130.7, 130.6, 130.5, 129.5, 129.1, 129.0, 128.9, 128.8, 128.6, 126.7, 126.2, 126.0, 124.9, 124.2, 123.6, 123.4, 120.0, 117.9, 96.7, 96.2, 88.6, 88.2, 30.8 ppm; MALDI-HRMS: *m/z* calcd for $C_{34}H_{20}O^+$: 444.1509 [$M^+$]; found: 444.1528.

*2-Acetyl-6,8-bis(phenylethynyl)pyrene (**12**)*: Prepared from **7** (1.21 g, 3 mmol), phenylacetylene (988 μL, 9 mmol), $[PdCl_2(PPh_3)_2]$ (421 mg, 0.6 mmol), $PPh_3$ (315 mg, 1.2 mmol), and CuI (114 mg, 0.6 mmol). The product was purified by column chromatography on silica gel using a gradient elution of 30→50% $CHCl_3$/petroleum ether. The combined fractions containing the product were evaporated and purified by column chromatography on silica gel using a gradient elution of 70→90% toluene/petroleum ether to give the product as a yellow solid (587 mg, 44%). $R_f=0.39$ (5% EtOAc/toluene); m.p. 221°C (50% $CHCl_3$/96% aq. EtOH); $^1$H NMR (300 MHz, $CDCl_3$): $\delta=8.55$ (s, 2H), 8.38 (d, $J=9.0$ Hz, 2H), 8.24 (s, 1H), 7.99 (d, $J=9.0$ Hz, 2H), 7.72–7.64 (m, 4H), 7.52–7.38 (m, 6H), 2.79 ppm (s, 3H); $^{13}$C NMR (300 MHz, $CDCl_3$): $\delta=198.6$, 134.8, 134.2 (2C), 132.4, 132.3 (4C), 131.3 (2C), 129.4 (2C), 129.0 (2C), 128.9 (4C), 126.4 (2C), 126.3, 125.6 (2C), 124.2, 123.5 (2C), 118.6 (2C), 96.1 (2C), 87.8 (2C), 27.2 ppm; MALDI-HRMS: *m/z* calcd for $C_{34}H_{20}O^+$: 444.1509 [$M^+$]; found: 444.1505.

*1-Acetyl-3,6,8-tris(phenylethynyl)pyrene (**13**)*: Prepared from **4** (1.44 g, 3 mmol), phenylacetylene (1.49 mL, 13.5 mmol), $[PdCl_2(PPh_3)_2]$ (632 mg, 0.9 mmol), $PPh_3$ (472 mg, 1.8 mmol), and CuI (171 mg, 0.9 mmol). The product was purified by column chromatography on silica gel using a gradient elution of 50→80% toluene/petroleum ether to give the product as a red solid (1.37 g, 84%). $R_f=0.63$ (5% EtOAc/toluene); m.p. 234°C (30% $CHCl_3$/ethanol); $^1$H NMR (300 MHz, $CDCl_3$): $\delta=8.88$ (d, $J=$ 9.3 Hz, 1H), 8.47–8.34 (m, 4H), 8.18 (s, 1H), 7.67–7.60 (m, 6H), 7.35–7.34 (m, 9H), 2.80 ppm (s, 3H); $^{13}$C NMR (300 MHz, $CDCl_3$): $\delta=201.0$, 133.9, 133.5, 132.1, 132.0, 131.8 (5C), 131.6 (2C), 131.3, 131.0, 130.7, 129.1, 128.6 (3C), 128.5 (5C), 127.8 (2C), 126.1, 126.0, 124.0, 123.4, 123.1, 122.7, 119.4, 119.2, 117.8, 96.4, 96.3, 96.2, 87.8, 87.6, 87.5, 29.7 ppm; MALDI-HRMS: *m/z* calcd for $C_{42}H_{24}O^+$: 544.1822 [$M^+$]; found: 544.1806.

*2-Acetyl-1,6,8-tris(phenylethynyl)pyrene (**14**)*: Prepared from **8** (1.44 g, 3 mmol), phenylacetylene (1.49 mL, 13.5 mmol), $[PdCl_2(PPh_3)_2]$ (632 mg, 0.9 mmol), $PPh_3$ (472 mg, 1.8 mmol), and CuI (171 mg, 0.9 mmol). The product was purified by column chromatography on silica gel using a gradient elution of 40→50% $CHCl_3$/petroleum ether. The combined fractions containing the product were evaporated and purified by repeated column chromatography on silica gel using a gradient elution of 80→100% toluene/petroleum ether to give the product as a brown solid (1.25 g, 77%). $R_f=0.50$ (5% EtOAc/toluene); m.p. 171–173°C ($CHCl_3$); $^1$H NMR (300 MHz, $CDCl_3$): $\delta=8.51$ (d, $J=9.0$ Hz, 1H), 8.36 (d, $J=$ 9.0 Hz, 1H), 8.32 (d, $J=9.3$ Hz, 1H), 8.25 (s, 1H), 8.16 (s, 1H), 7.85 (d, $J=9.3$ Hz, 1H), 7.65–7.61 (m, 6H), 7.38–7.34 (m, 9H), 2.92 ppm (s, 3H); $^{13}$C NMR (300 MHz, $CDCl_3$): $\delta=201.2$, 139.0, 133.8, 132.4, 131.8, 131.7–131.5 (8C), 131.4, 130.2, 128.9, 128.6, 128.5–128.4 (6C), 126.9, 126.6, 126.5, 125.4, 125.3, 124.6, 123.2, 123.1, 123.0, 118.7, 118.6, 116.1, 101.7, 96.1, 96.0, 87.5, 87.4, 87.3, 30.5 ppm; MALDI-HRMS: *m/z* calcd for $C_{42}H_{24}O^+$: 544.1822 [$M^+$]; found: 545.1907).

**General procedure for haloform oxidation**: Sodium hydroxide (870 mg, 22 mmol) was dissolved in water (12 mL). The solution was cooled to 0°C and bromine (308 μL, 6 mmol) was added. After stirring for 10 min at RT, the resulting yellow solution was diluted with 1,4-dioxane (12 mL),

 © 2008 Wiley-VCH Verlag GmbH & Co. KGaA, Weinheim 

and the corresponding ketone (1 mmol) was added in five portions over a period of 10 min. The solution was stirred at 0 °C for 3 h and then left overnight at RT. Saturated $Na_2SO_3$ (2 mL) was added, and the mixture stirred at RT for 1 h. After acidification with 1 M aq. citric acid (to pH 3–4), the reaction mixture was transferred into a separating funnel and extracted three times with $CHCl_3$. The combined organic phases were dried over $Na_2SO_4$ and evaporated. Recrystallization from the solvents mentioned below in each case gave analytical-quality samples of the compounds, whereas the main portions of the products were used directly in the next step without further purification.

*3-Phenylethynylpyrene-1-carboxylic acid (**15**)*: By using the general procedure, **9** (344 mg, 1 mmol) was converted into the title product (yellow solid; 342 mg, 95%). $R_f$=0.60 (5% MeOH/$CH_2Cl_2$); m.p. >250 °C (1% DMF/$MeNO_2$); MALDI-HRMS: *m/z* calcd for $C_{25}H_{14}O_2^+$: 346.0989 [$M^+$]; found: 346.0991.

*6-Phenylethynylpyrene-2-carboxylic acid (**16**)*: Prepared from **10** (344 mg, 1 mmol) to give the title compound as a yellow solid (331 mg, 92%). $R_f$= 0.48 (5% MeOH/$CH_2Cl_2$); m.p. >250 °C (1% DMF/$MeNO_2$); MALDI-HRMS: *m/z* calcd for $C_{25}H_{14}O_2^+$: 346.0989 [$M^+$]; found: 346.0988.

*3,6-Bis(phenylethynyl)pyrene-1-carboxylic acid (**17**)*: Prepared from **11** (444 mg, 1 mmol) to give the title compound as an orange solid (420 mg, 94%). $R_f$=0.60 (5% MeOH/$CH_2Cl_2$); m.p. >250 °C (1% DMF/$MeNO_2$); MALDI-HRMS: *m/z* calcd for $C_{33}H_{18}O_2^+$: 446.1301 [$M^+$]; found: 446.1303.

*6,8-Bis(phenylethynyl)pyrene-2-carboxylic acid (**18**)*: Prepared from **12** (444 mg, 1 mmol) to give the title compound as a yellow solid (402 mg, 90%). $R_f$=0.41 (5% MeOH/$CH_2Cl_2$); m.p. >250 °C (1% DMF/$MeNO_2$); MALDI-HRMS: *m/z* calcd for $C_{33}H_{18}O_2^+$: 446.1301 [$M^+$]; found: 446.1305.

*3,6,8-Tris(phenylethynyl)pyrene-1-carboxylic acid (**19**)*: By using the general procedure, **13** (545 mg, 1 mmol) was converted into the title compound (red solid; 544 mg, 99%). $R_f$=0.50 (5% MeOH/$CH_2Cl_2$); m.p. >250 °C (1% DMF/$MeNO_2$); MALDI-HRMS: *m/z* calcd for $C_{41}H_{22}O_2^+$: 546.1614 [$M^+$]; found: 546.1615.

*3,6,8-Tris(phenylethynyl)pyrene-2-carboxylic acid (**20**)*: Prepared from **14** (545 mg, 1 mmol) to give the title compound as a red solid (502 mg, 92%). $R_f$=0.40 (5% MeOH/$CH_2Cl_2$); m.p. 163–166 °C (1% DMF/$MeNO_2$); MALDI-HRMS: *m/z* calcd for $C_{41}H_{22}O_2^+$: 546.1614 [$M^+$]; found: 546.1610.

**General procedure for the preparation of compounds 22a–f**: Diisopropylethylamine (132 μL, 0.76 mmol) was added as one portion to a stirred solution of the corresponding acid (0.39 mmol) and HBTU (137 mg, 0.36 mmol) in DMF (3 mL) (**15**, **16**) or DMF (2 mL) and 1,1-dichloroethane (1 mL) (**17**–**20**). The mixture was stirred for 10 min at RT and then added dropwise to a stirred solution of **21**[16] (200 mg, 0.35 mmol) in DMF (3 mL). After stirring for 1.5 h, TLC monitoring showed that the reaction was complete. The reaction mixture was diluted with $CH_2Cl_2$ (100 mL) and washed with water (2×150 mL), 5% $NaHCO_3$ (2× 150 mL), and water (3×150 mL). The organic layer was dried over $Na_2SO_4$ and evaporated. The residue was purified by column chromatography on silica gel using a gradient elution of 1:5→30% $Et_3N$/acetone/toluene.

*(1R,3R,4R,7S)-1-(4,4′-Dimethoxytrityloxymethyl)-7-hydroxy-5-(3-phenylethynylpyren-1-carbonyl)-3-(thymin-1-yl)-2-oxa-5-azabicyclo[2.2.1]heptane (**22a**)*: Prepared from **15** (135 mg) to give the title compound as an orange foam (rotameric mixture ≈1:0.5 by $^1$H NMR; 214 mg, 68%). $R_f$ 0.33 (1:50% $NEt_3$/acetone/toluene); $^1$H NMR (300 MHz, [$D_6$]DMSO; the signals are given for the major rotamer): δ=1.60 (br s, 1H), 8.77 (d, *J*= 9.0 Hz, 1H), 8.56–8.50 (m, 3H), 8.46–8.39 (m, 2H), 8.30–8.25 (m, 2H), 7.92–7.88 (m, 2H), 7.65–7.56 (m, 5H), 7.48–7.25 (m, 8H), 7.05–7.02 (m, 4H), 6.36 (d, *J*=3.6 Hz, 1H), 6.02 (s, 1H), 5.26 (s, 1H), 4.29 (d, *J*= 4.2 Hz, 1H), 3.81 (s, 6H), 3.70 (d, *J*=11.0 Hz, 1H), 3.60 (d, *J*=11.0 Hz, 1H), 3.45–3.26 (m, 2H, partial overlap with $H_2O$), 1.51 ppm (s, 3H); $^{13}$C NMR (75 MHz, [$D_6$]DMSO; the signals are given for the major rotamer): δ=169.2, 164.8, 159.2 (2C), 150.9, 145.6, 136.3, 136.0, 135.9, 135.8, 132.6, 132.5, 132.4, 132.2, 131.5 (2C), 131.4, 130.8 (2C), 130.7 (2C), 130.5, 129.9 (2C), 129.8 (2C), 128.9 (2C), 128.8 (2C), 128.7 (2C), 128.0, 127.8, 127.6, 125.7, 124.7, 124.3, 123.2, 117.6, 114.3 (4C), 109.2, 96.5, 88.8, 88.5, 86.7, 86.6, 69.9, 66.0, 60.2, 56.0 (2C), 52.3, 13.3 ppm; MALDI-HRMS: *m/z* calcd for $C_{57}H_{45}N_3O_8Na^+$: 922.3090 [$M^+$+Na]; found: 922.3137.

*(1R,3R,4R,7S)-1-(4,4′-Dimethoxytrityloxymethyl)-7-hydroxy-5-(6-phenylethynylpyren-2-carbonyl)-3-(thymin-1-yl)-2-oxa-5-azabicyclo[2.2.1]heptane (**22b**)*: Prepared from **16** (135 mg) to give the title compound as a yellow foam (rotameric mixture ≈9:1 by $^1$H NMR; 284 mg, 90%). $R_f$=0.44 (1:50% $NEt_3$/acetone/toluene); $^1$H NMR (300 MHz, [$D_6$]DMSO; the signals are given for the major rotamer): δ=11.34 (br s, 1H), 8.74–8.10 (m, 8H), 7.73–7.15 (m, 15H), 6.90–6.84 (m, 4H), 6.01 (s, 1H), 5.93 (d, *J*= 3.6 Hz, 1H), 4.46 (s, 1H), 4.14–4.12 (m, 1H), 3.88 (s, 6H), 3.71–3.40 (m, 4H, partial overlap with $H_2O$), 1.39 ppm (s, 3H); $^{13}$C NMR (75 MHz, [$D_6$]DMSO; the signals are given for the major rotamer): δ=169.0, 161.2, 158.1 (2C), 150.2, 144.5, 135.2, 134.9, 134.1, 133.5, 132.7, 132.4, 132.1, 131.5 (2C), 130.9, 130.4, 130.1, 130.0, 129.7 (2C), 129.1, 128.9, 128.8 (2C), 128.4, 127.9 (2C), 127.6 (2C), 126.8 (2C), 125.3 (2C), 124.7, 124.4, 123.8, 122.8, 120.4, 120.0, 113.2 (4C), 108.6, 97.7, 89.0, 87.9, 86.7, 85.8, 69.0, 67.5, 66.8, 65.9, 54.9 (2C), 12.2 ppm; MALDI-HRMS: *m/z* calcd for $C_{57}H_{45}N_3O_8Na^+$: 922.3135 [$M^+$+Na]; found: 922.309).

*(1R,3R,4R,7S)-1-(4,4′-Dimethoxytrityloxymethyl)-7-hydroxy-5-[3,6-bis(phenylethynyl)pyren-1-carbonyl]-3-(thymin-1-yl)-2-oxa-5-azabicyclo[2.2.1]heptane (**22c**)*: Prepared from **17** (174 mg) to give the title compound as an orange foam (rotameric mixture ≈1:0.2:0.9 by $^1$H NMR; 262 mg, 75%). $R_f$=0.49 (1:60% $NEt_3$/acetone/toluene); $^1$H NMR (300 MHz, [$D_6$]DMSO; the signals are given for the major rotamer): δ= 11.45 (br s, 1H), 8.78–8.68 (m, 1H), 8.48–8.34 (m, 3H), 7.82–7.80 (m, 1H), 7.67–7.49 (m, 17H), 7.39–7.16 (m, 5H), 6.96–6.92 (m, 4H), 6.30 (d, *J*=3.9 Hz, 1H), 5.98 (s, 1H), 5.31 (s, 1H), 4.23 (d, *J*=4.5 Hz, 1H), 3.87 (s, 6H), 3.71–3.60 (m, 2H), 3.41–3.20 (m, 2H, partial overlap with $H_2O$), 1.43 ppm (s, 3H); $^{13}$C NMR (75 MHz, [$D_6$]DMSO; the signals are given for the major rotamer): δ=169.1, 164.8, 159.2 (2C), 150.9, 145.6, 136.3 (2C), 136.0, 135.9 (2C), 135.8, 134.3, 133.0 (2C), 132.9 (2C), 132.7 (2C), 132.6 (2C), 132.5 (2C), 132.3 (2C), 131.8, 130.8 (2C), 130.6 (2C), 129.8 (2C), 129.7 (2C), 129.5 (2C), 129.1 (2C), 128.6 (3C), 124.2 (2C), 123.2 (2C), 119.1, 114.3 (4C), 109.2, 97.1, 97.0, 88.9, 88.4, 87.4, 87.0, 86.7, 70.0, 66.0, 60.2, 56.0 (2C), 46.6, 13.2 ppm; ESI-HRMS: *m/z* calcd for $C_{65}H_{49}N_3O_8Na^+$: 1022.3412 [$M^+$+Na]; found: 1022.3365.

*(1R,3R,4R,7S)-1-(4,4′-Dimethoxytrityloxymethyl)-7-hydroxy-5-[6,8-bis(phenylethynyl)pyren-2-carbonyl]-3-(thymin-1-yl)-2-oxa-5-azabicyclo[2.2.1]heptane (**22d**)*: Prepared from **18** (174 mg) to give the title compound as an orange foam (rotameric mixture ≈1:3.3 by $^1$H NMR; 227 mg, 65%). $R_f$=0.43 (1:50% $NEt_3$/acetone/toluene); $^1$H NMR (300 MHz, [$D_6$]DMSO; the signals are given for the major rotamer): δ= 11.41 (br s, 1H), 8.84–8.55 (m, 3H), 8.35 (s, 1H), 7.87–7.83 (m, 2H), 7.69–7.55 (m, 19H), 7.38 (d, *J*=8.7 Hz, 2H), 6.99–6.96 (m, 4H), 6.14 (s, 1H), 6.05–6.03 (m, 1H), 4.56 (s, 1H), 4.28 (br s, 1H), 3.85 (d, *J*=11.7 Hz, 1H), 3.80 (s, 6H), 3.62–3.51 (m, 3H), 1.50 ppm (s, 3H); $^{13}$C NMR (75 MHz, [$D_6$]DMSO; the signals are given for the major rotamer): δ=169.8, 164.6, 159.2 (2C), 151.2, 145.6, 136.3, 135.9, 134.3, 134.2 (2C), 134.0, 132.9 (4C), 132.8 (4C), 132.6 (2C), 132.5 (2C), 132.3 (2C), 130.0 (2C), 129.9 (2C), 129.7 (4C), 129.6 (4C), 128.9, 128.6, 127.8, 127.2, 126.2, 123.0, 118.2, 114.3 (4C), 109.6 (2C), 96.8 (2C), 88.0, 87.2, 86.7, 80.1 (2C), 70.1, 67.1, 56.0 (2C), 52.9, 13.3 ppm. ESI-HRMS: *m/z* calcd for $C_{65}H_{49}N_3O_8Na^+$: 1022.3412 [$M^+$+Na]; found: 1022.3402.

*(1R,3R,4R,7S)-1-(4,4′-Dimethoxytrityloxymethyl)-7-hydroxy-5-[3,6,8-tris(phenylethynyl)pyren-1-carbonyl]-3-(thymin-1-yl)-2-oxa-5-azabicyclo[2.2.1]heptane (**22e**)*: Prepared from **19** (213 mg) to give the title compound as an orange foam (304 mg, 62%). $R_f$=0.25 (1:50% $NEt_3$/acetone/toluene); $^1$H NMR (500 MHz, [$D_6$]DMSO; the signals are given for the major rotamer): δ=11.50 (br s, 1H, exchange with $D_2O$), 8.90–8.74 (m, 4H), 8.56 (s, 1H), 8.38–8.36 (m, 1H), 7.86–7.82 (m, 5H), 7.54–7.47 (m, 11H), 7.38–7.14 (m, 9H), 6.96–6.94 (m, 4H), 6.26 (d, *J*=3.5 Hz, 1H), 5.94 (s, 1H), 5.18 (s, 1H), 4.20 (d, *J*=2.5 Hz, 1H), 3.77 (s, 6H), 3.59 (d, *J*=10.0 Hz, 1H), 3.49 (d, *J*=11.0 Hz, 1H), 3.27–3.22 (m, 2H, partial overlap with $H_2O$), 1.41 ppm (s, 3H); $^{13}$C NMR (125 MHz, [$D_6$]DMSO; the signals are given for the major rotamer): δ=168.7, 164.8, 159.2 (2C), 150.9, 145.6, 136.3 (2C), 136.0, 135.9 (2C), 135.8, 135.3, 134.8, 134.1 (2C), 133.5 (2C), 132.7 (2C), 132.6 (4C), 132.5, 132.4, 132.3, 131.9 (2C), 130.8

 © 2008 Wiley-VCH Verlag GmbH & Co. KGaA, Weinheim 

(2C), 130.7 (2C), 130.5, 130.3, 129.8 (4C), 129.7, 128.9, 128.7, 128.6, 128.5, 127.6 (2C), 124.4, 124.3, 124.1, 123.0 (2C), 122.9, 119.0, 114.3 (4C), 109.6, 109.2, 97.7, 97.6, 97.5, 97.3, 88.8, 88.0, 86.8, 69.9, 66.0, 60.2, 55.9 (2C), 52.4, 13.5 ppm; ESI-HRMS: *m/z* calcd for $C_{73}H_{53}N_5O_8Na^+$: 1122.3724 [$M^+$+Na]; found: 1122.3719.

*(1R,3R,4R,7S)-1-(4,4′-Dimethoxytrityloxymethyl)-7-hydroxy-5-[3,6,8-tris-(phenylethynyl)pyren-1-carbonyl]-3-(thymin-1-yl)-2-oxa-5-azabicyclo-[2.2.1]heptane (**22f**)*: Prepared from **20** (213 mg) to give the title compound as an orange foam (rotameric mixture ≈1:0.9:0.5 by $^1$H NMR; 162 mg, 42%). $R_f$ 0.30 (1:60% $NEt_3$/acetone/toluene); $^1$H NMR (300 MHz, [D$_6$]DMSO; the signals are given for the major rotamer): $\delta$ = 11.06 (br s, 1H), 8.71–8.52 (m, 2H), 7.97–7.92 (m, 3H), 7.84–7.77 (m, 2H), 7.67–7.29 (m, 24H), 7.06–7.03 (m, 4H), 5.95 (s, 1H), 5.91 (d, $J$ = 3.9 Hz, 1H), 4.25–4.23 (m, 1H), 4. 11 (s, 1H) 3.88 (s, 6H), 3.84–3.80 (m, 2H), 3.69–3.59 (m, 2H), 1.49 ppm (s, 3H); $^{13}$C NMR (75 MHz, [D$_6$]DMSO; the signals are given for the major rotamer): $\delta$ = 167.8, 164.5, 159.2 (2C), 150.9, 145.6, 136.3 (2C), 136.0, 135.9, 135.8, 134.0, 132.7 (4C), 132.5 (2C), 132.4, 132.3 (2C), 131.9 (2C), 130.7 (4C), 129.9 (4C), 129.7, 129.6, 129.5, 129.0 (2C), 128.9 (2C), 128.6 (2C), 127.8, 127.6, 127.5, 124.4, 124.3, 124.1, 123.0, 122.9, 119.4, 119.3, 119.2, 119.1, 119.0, 114.3 (4C), 109.7, 109.5, 97.7, 97.6, 97.5, 97.4, 88.4, 88.1, 86.8, 68.3, 66.0, 60.2, 56.0 (2C), 52.0, 11.7 ppm; ESI-HRMS: *m/z* calcd for $C_{73}H_{53}N_3O_8Na^+$: 1122.3724 [$M^+$+Na]; found: 1122.3710.

**General procedure for the preparation of compounds 23a–f**: The relevant LNA nucleoside derivative (0.2 mmol) was evaporated with dry $CH_2Cl_2$ (2×30 mL), dissolved in anhydrous $CH_2Cl_2$ (20 mL), then diisopropylammonium tetrazolide (52 mg, 0.3 mmol) and bis(*N*,*N*-diisopropylamino)-2-cyanoethoxyphosphine (96μL, 0.3 mmol) were added under argon and the resulting mixture was stirred for 12 h. The mixture was then diluted with $CH_2Cl_2$ (100 mL) and washed with saturated aqueous solutions of $NaHCO_3$ (2×100 mL) and brine (100 mL). The organic layer was dried over $Na_2SO_4$ and evaporated, and the crude material was purified by chromatography on silica gel eluted with 1:30% $NEt_3$/acetone/toluene.

*(1R,3R,4R,7S)-7-(2-Cyanoethoxy(diisopropylamino)phosphinoxy)-1-(4,4′-dimethoxytrityloxymethyl)-7-hydroxy-5-(3-phenylethynylpyren-1-carbonyl)-3-(thymin-1-yl)-2-oxa-5-azabicyclo[2.2.1]heptane (**23a**)*: Yellow foam (202 mg, 92%). $R_f$ = 0.52, 0.48 (1:50% $NEt_3$/acetone/toluene); $^{31}$P NMR (120 MHz, [D$_6$]DMSO): $\delta$ = 149.20, 149.17 ppm (1:1); MALDI-HRMS: *m/z* calcd for $C_{66}H_{62}N_5O_9PNa^+$: 1122.4177 [$M^+$+Na]; found: 1122.4170.

*(1R,3R,4R,7S)-7-(2-Cyanoethoxy(diisopropylamino)phosphinoxy)-1-(4,4′-dimethoxytrityloxymethyl)-7-hydroxy-5-(6-phenylethynylpyren-2-carbonyl)-3-(thymin-1-yl)-2-oxa-5-azabicyclo[2.2.1]heptane (**23b**)*: Yellow foam (188 mg, 85%). $R_f$ = 0.46, 0.42 (1:50% $NEt_3$/acetone/toluene); $^{31}$P NMR (120 MHz, [D$_6$]DMSO): $\delta$ = 150.89, 149.12 ppm (1:1.3); MALDI-HRMS: *m/z* calcd for $C_{66}H_{62}N_5O_9PNa^+$: 1122.4177 [$M^+$+Na]; found: 1122.4194.

*(1R,3R,4R,7S)-7-(2-Cyanoethoxy(diisopropylamino)phosphinoxy)-1-(4,4′-dimethoxytrityloxymethyl)-7-hydroxy-5-[3,6-bis(phenylethynyl)pyren-1-carbonyl]-3-(thymin-1-yl)-2-oxa-5-azabicyclo[2.2.1]heptane (**23c**)*: Orange foam (216 mg, 90%). $R_f$ = 0.39, 0.37 (1:30% $NEt_3$/acetone/toluene); $^{31}$P NMR (120 MHz, [D$_6$]DMSO; the signals for the major rotamer are given): $\delta$ = 148.96, 147.77 ppm (1:1); MALDI-HRMS: *m/z* calcd for $C_{74}H_{66}N_5O_9PNa^+$: 1222.4490 [$M^+$+Na]; found: 1222.4484.

*(1R,3R,4R,7S)-7-(2-Cyanoethoxy(diisopropylamino)phosphinoxy)-1-(4,4′-dimethoxytrityloxymethyl)-7-hydroxy-5-[6,8-bis(phenylethynyl)pyren-2-carbonyl]-3-(thymin-1-yl)-2-oxa-5-azabicyclo[2.2.1]heptane (**23d**)*: Orange foam (237 mg, 97%). $R_f$ = 0.59 (1:50% $NEt_3$/acetone/toluene); $^{31}$P NMR (120 MHz, [D$_6$]DMSO; the signals are given for the major rotamer): $\delta$ = 149.13, 147.90 ppm (1:2.2); ESI-HRMS: *m/z* calcd for $C_{74}H_{66}N_5O_9PNa^+$: 1222.4490 [$M^+$+Na] found: 1222.4468.

*(1R,3R,4R,7S)-7-(2-Cyanoethoxy(diisopropylamino)phosphinoxy)-1-(4,4′-dimethoxytrityloxymethyl)-7-hydroxy-5-[3,6,8-tris(phenylethynyl)pyren-1-carbonyl]-3-(thymin-1-yl)-2-oxa-5-azabicyclo[2.2.1]heptane (**23e**)*: Orange foam (247 mg, 95%). $R_f$ = 0.44, 0.42 (1:50% $NEt_3$/acetone/toluene); $^{31}$P NMR (120 MHz, [D$_6$]DMSO): $\delta$ = 149.69, 148.07 ppm (1:1.2); ESI-HRMS: *m/z* calcd for $C_{82}H_{70}N_5O_9PNa^+$: 1322.4803 [$M^+$+Na]; found: 1322.4842.

*(1R,3R,4R,7S)-7-(2-Cyanoethoxy(diisopropylamino)phosphinoxy)-1-(4,4′-dimethoxytrityloxymethyl)-7-hydroxy-5-[3,6,8-tris(phenylethynyl)pyren-2-carbonyl]-3-(thymin-1-yl)-2-oxa-5-azabicyclo[2.2.1]heptane (**23f**)*: Orange foam (231 mg, 89%). $R_f$ = 0.53, 0.48 (1:50% $NEt_3$/acetone/toluene); $^{31}$P NMR (120 MHz, [D$_6$]DMSO): $\delta$ = 149.02, 147.81 ppm (1:0.4); ESI-HRMS: *m/z* calcd for $C_{82}H_{70}N_5O_9PNa^+$: 1322.4803 [$M^+$+Na]; found: 1322.4813.

## Acknowledgements

We greatly appreciate funding from the Danish National Research Foundation and the Sixth Framework Programme Marie Curie Host Fellowships for Early Stage Research Training under contract number MEST-CT-2004-504018. I.V.A. and V.A.K. acknowledge support from the Russian Foundation for Basic Research (RFBR), grant number 06-03-32426.

[1] a) J. R. Lakowicz, *Principles of Fluorescence Spectroscopy*, 3rd ed., Springer, Singapore, **2006**; b) F. M. Winnik, *Chem. Rev.* **1993**, *93*, 587–614.

[2] For some recent examples, see: a) K. Yamana, R. Iwase, S. Furutani, H. Tsuchida, H. Zako, T. Yamaoka, A. Murakami, *Nucleic Acids Res.* **1999**, *27*, 2387–2392; b) K. Yamana, H. Zako, K. Asazuma, R. Iwase, H. Nakano, A. Murakami, *Angew. Chem.* **2001**, *113*, 1138–1140; *Angew. Chem. Int. Ed.* **2001**, *40*, 1104–1106; c) V. A. Korshun, D. A. Stetsenko, M. J. Gait, *J. Chem. Soc. Perkin Trans. 1* **2002**, 1092–1104; d) N. N. Dioubankova, A. D. Malakhov, D. A. Stetsenko, M. J. Gait, P. E. Volynsky, R. G. Efremov, V. A. Korshun, *ChemBioChem* **2003**, *4*, 841–847; e) K. Kawai, H. Yoshida, T. Takada, S. Tojo, T. Majima, *J. Phys. Chem. B* **2004**, *108*, 13547–13550; f) M. Nakamura, Y. Fukunaga, K. Sasa, Y. Ohtoshi, K. Kanaori, H. Hayashi, H. Nakano, K. Yamana, *Nucleic Acids Res.* **2005**, *33*, 5887–5895; g) D. S. Novopashina, D. A. Stetsenko, O. S. Totskaya, M. N. Repkova, A. G. Venyaminova, *Nucleosides Nucleotides Nucleic Acids* **2005**, *24*, 729–734; h) T. S. Kumar, J. Wengel, P. J. Hrdlicka, *ChemBioChem* **2007**, *8*, 1122–1125; i) I. Van Daele, N. Bomholt, V. V. Filichev, S. Van Calenbergh, E. B. Pedersen, *ChemBioChem* **2008**, *9*, 791–801; j) D. Honcharenko, C. Zhou, J. Chattopadhyaya, *J. Org. Chem.* **2008**, *73*, 2829–2842; k) M. Nakamura, Y. Murakami, K. Sasa, H. Hayashi, K. Yamana, *J. Am. Chem. Soc.* **2008**, *130*, 6904–6905.

[3] P. J. Hrdlichka, B. R. Babu, M. D. Sørensen, N. Harrit, J. Wengel, *J. Am. Chem. Soc.* **2005**, *127*, 13293–13299.

[4] a) S. K. Singh, R. Kumar, J. Wengel, *J. Org. Chem.* **1998**, *63*, 10035–10039; b) M. D. Sørensen, M. Petersen, J. Wengel, *Chem. Commun.* **2003**, 2130–2131; c) N. Karla, B. R. Babu, V. S. Parmar, J. Wengel, *Org. Biomol. Chem.* **2004**, *2*, 2885–2887; d) B. R. Babu, P. J. Hrdlichka, C. J. McKenzie, J. Wengel, *Chem. Commun.* **2005**, 1705–1706; e) B. R. Babu, D. Lindegaard, T. S. Kumar, J. Maity, I. V. Astakhova, A. D. Malakhov, M. Sørensen, N. Karla, V. A. Korshun, P. J. Hrdlichka, A. K. Prasad, V. S. Parmar, J. Wengel, unpublished results.

[5] D. Lindegaard, A. S. Madsen, I. V. Astakhova, A. D. Malakhov, B. R. Babu, V. A. Korshun, J. Wengel, *Bioorg. Med. Chem.* **2008**, *16*, 94–99.

[6] P. J. Hrdlichka, B. R. Babu, M. D. Sørensen, J. Wengel, *Chem. Commun.* **2004**, 1478–1479.

[7] T. Umemoto, P. J. Hrdlicka, B. R. Babu, J. Wengel, *ChemBioChem* **2007**, *8*, 2240–2248.

[8] J. Wengel, *Org. Biomol. Chem.* **2004**, *2*, 277–280.

[9] a) H. Maeda, T. Maeda, K. Mizuno, K. Fujimoto, H. Shimizu, M. Inouye, *Chem. Eur. J.* **2006**, *12*, 824–831; b) A. C. Benniston, A. Harriman, S. L. Howell, C. A. Sams, Y.-G. Zhi, *Chem. Eur. J.* **2007**, *13*, 4665–4674.

[10] a) V. A. Korshun, I. A. Prokhorenko, S. V. Gontarev, M. V. Skorobogatyi, K. V. Balakin, E. V. Manasova, A. D. Malakhov, Y. A. Berlin, *Nucleosides Nucleotides* **1997**, *16*, 1461–1464; b) A. D. Malakhov, M. V. Skorobogatyi, I. A. Prokhorenko, S. V. Gontarev, D. T. Koz-

 © 2008 Wiley-VCH Verlag GmbH & Co. KGaA, Weinheim 

hich, D. A. Stetsenko, I. A. Stepanova, Z. O. Shenkarev, Y. A. Berlin, V. A. Korshun, *Eur. J. Org. Chem.* **2004**, 1298–1307; c) N. N. Dioubankova, A. D. Malakhov, Z. O. Shenkarev, V. A. Korshun, *Tetrahedron* **2004**, *60*, 4617–4626; d) I. A. Prokhorenko, A. D. Malakhov, A. A. Kozlova, K. Momynaliev, V. M. Govorun, V. A. Korshun, *Mutat. Res.* **2006**, *599*, 144–151; e) I. V. Astakhova, A. D. Malakhov, I. A. Stepanova, A. V. Ustinov, S. L. Bondarev, A. S. Paramonov, V. A. Korshun, *Bioconjugate Chem.* **2007**, *18*, 1972–1980.

[11] J. Grimshaw, J. Trocha-Grimshaw, *J. Chem. Soc. Perkin Trans. 1* **1972**, 1622–1623.

[12] K. Ogino, S. Iwashima, H. Inokuchi, Y. Harada, *Bull. Chem. Soc. Jpn.* **1965**, *38*, 473–477.

[13] R. G. Harvey, M. Konieczny, J. Pataki, *J. Org. Chem.* **1983**, *48*, 2930–2932.

[14] a) K. Sonogashira, Y. Tohda, N. Hagihara, *Tetrahedron Lett.* **1975**, *16*, 4467–4470; b) K. Sonogashira, *Metal-Catalyzed Cross-Coupling Reactions* (Eds.: F. Diederich, P. J. Stang), Wiley-VCH, New York, **1998**, 203–229.

[15] a) W. C. Trahanovsky, *Oxidation in Organic Chemistry, Part C*, Academic Press, New York, **1978**, chapter 5; b) A. Okamoto, K. Tainaka, K. Nishiza, I. Saito, *J. Am. Chem. Soc.* **2005**, *127*, 13128–13129.

[16] a) C. Rosenbohm, S. M. Christensen, M. D. Sørensen, D. S. Pedersen, L. Larsen, J. Wengel, T. Koch, *Org. Biomol. Chem.* **2003**, *1*, 655–663; b) S. M. Christensen, C. Rosenbohm, M. Sørensen, L. Larsen, J. Wengel, T. Koch, *Nucleosides Nucleotides Nucleic Acids* **2003**, *22*, 1131–1133.

[17] L. A. Carpino, H. Imazumi, A. El-Faham, F. J. Ferrer, C. Zhang, Y. Lee, B. M. Foxman, P. Henklein, C. Hanay, C. Mügge, H. Wenschuh, J. Klose, M. Beyermann, M. Bienert, *Angew. Chem.* **2002**, *114*, 457–461; *Angew. Chem. Int. Ed.* **2002**, *41*, 441–445.

[18] K. E. Nielsen, S. K. Singh, J. Wengel, J. P. Jakobsen, *Bioconjugate Chem.* **2000**, *11*, 228–238.

[19] A. A. Koshkin, S. K. Singh, P. Nielsen, V. K. Rajwanshi, R. Kumar, M. Meldgaard, C. E. Olsen, J. Wengel, *Tetrahedron* **1998**, *54*, 3607–3630.

[20] J. V. Morris, M. A. Mahaney, J. R. Huber, *J. Phys. Chem.* **1976**, *80*, 969–974.

[21] V. A. Korshun, E. V. Manasova, K. V. Balakin, I. A. Prokhorenko, A. G. Buchatskii, Y. A. Berlin, *Russ. J. Bioorg. Chem.* **1996**, *22*, 807–809.

[22] N. Nijegorodov, R. Mabbs, W. S. Downey, *Spectrochim. Acta, Part A* **2001**, *57*, 2673–2685.

[23] S. T. Gaballah, Y. H. A. Hussein, N. Anderson, T. T. Lian, T. L. Netzel, *J. Phys. Chem. A* **2005**, *109*, 10832–10854.

[24] D. Auld, A. Simeonov, *Assay Drug Dev. Technol.* **2005**, *3*, 581–582.

[25] J. B. Birks, *Rep. Prog. Phys.* **1975**, *38*, 903–974.

[26] R. G. Harvey, M. Konieczny, J. Pataki, *J. Org. Chem.* **1983**, *48*, 2930–2932.

[27] M. H. Caruthers, A. D. Barone, S. L. Beaucage, D. R. Dodds, E. F. Fisher, L. J. McBride, M. Matteucci, Z. Stabinsky, J.-Y. Tang, *Methods Enzymol.* **1987**, *154*, 287–313.

Received: June 3, 2008
Published online: October 31, 2008

 © 2008 Wiley-VCH Verlag GmbH & Co. KGaA, Weinheim 